PART-C

Designing of catalysts based on Palladium & Phosphomolybdic acid

CHAPTER 1

Cesium salt of palladium substituted phosphomolybdate ($PMo_{11}Pd$): Synthesis, characterization and application for hydrogenation of Levulinic acid

As described in the general introduction as well as chapter 2 (Part A), transition metal substituted polyoxometalates (TMSPOMs) have gained more attention for various applications in interdisciplinary fields like medicine, magneto chemistry, electrochemical, materials science and catalysis, as they consist the advantages of the both transition metal and POMs [1-4]. In this direction, number of articles have been reported using precious noble transition metals (Ru, Rh, Ir, Os and Pt) substituted polyoxometalates [5-33]. At the same time, only four reports [34-37] are available on Pd substituted polyoxometalates and that is based on phosphotungstate, even though, historically and currently palladium (Pd) has been dominated over other metals as central tool for numerous organic transformations [38, 39].

In 2002, Neumann et al. reported potassium salt of palladium substituted phosphotungstic acid [$K_5(PdPW_{11}O_{39}).12H_2O$] and its catalytic activity evaluated for the Suzuki-Miyaura cross-coupling reaction using chlorobenzene and phenylboronic acid in ethanol–water solvent system at 85 °C in 12 h to achieved 99% yield of biphenyl [34]. In present article synthesized catalyst [$K_5(PdPW_{11}O_{39}).12H_2O$] was also supported on γ-Al_2O_3 to make heterogeneous in nature and applied as a heterogeneous catalyst for the same reaction under the solvent free condition at 130 °C for 16 h to achieve 99% conversion of biphenyl. In same year, same group, reported potassium salt of palladium substituted phosphotungstic acid supported on activated carbon [$K_5(PdPW_{11}O_{39}).12H_2O/C$]. Its catalytic activity was evaluated for hydrogenation of aromatic ketones [35]. After almost 11 years, in 2013 Parida et al. reported synthesis of palladium substituted phosphotungstate supported on mesoporous silica (50LPdW/MCM-41) for hydrogenation of p-nitrophenol to p-aminophenol at room temperature [36].

Recently, in 2022 Yan group reported synthesis of solubilized single-atom sites polyoxometalate-supported catalyst, tetrammonium salt of $PMo_{11}O_{39}Pd_1$, $PMo_{11}O_{39}Pt_1$, and $PMo_{11}O_{39}Rh_1$ [37]. The synthesized catalyst was used to study the effect of spillover hydrogen on catalyst during the reaction. They found a

unique interplay between positively charged Pd and a reducible Mo-based support for hydrogen spillover. To confirm this kinetics with poisoning studies were carried out using in-situ characterization techniques as well as DFT calculation.

Thus, literature survey shows that only one reports are available on palladium substituted phosphomolybdate. Keeping this in mind, we have synthesized $PMo_{11}Pd$, characterized and evaluated it for hydrogenation of styrene and cyclohexene under optimized conditions viz., (i) catalyst (5 mg) styrene (10 mmol), EtOH: H_2O (30:20 mL), H_2 pressure (5 bar), time (3 h), temperature (30 °C) and (ii) catalyst amount (25 mg), cyclohexene (9.87 mmol), H_2O (50 mL), H_2 pressure (10 bar), time (2 h) and temperature (50 °C) as described in chapter 1 and 2 of part A respectively. The obtained results (99% and 96% conversion respectively) made as to explore its activity for hydrogenation of bio-mass derived levulinic acid (LA) using formic acid (FA) as internal hydrogen source, because of immense importance of its hydrogenated product as mentioned in part B chapter 2. A literature study shows that only few reports are available on Pd catalyzed LA hydrogenation using FA and H_2 but they suffered from aggregate formation during the synthesis or during its utilization [40-50]. Therefore, stabilization of Pd nanoparticles is essential.

In this context, in the present chapter we are reporting designing of cesium salt of palladium substituted phosphomolybdate via One-pot method. The synthesized catalyst was systematically characterized by various physicochemical techniques such as EDX, TGA, FT-IR, ^{31}P MAS NMR, XPS, powder XRD, TEM, HRTEM and STEM analysis. The catalyst efficiency was evaluated for solvent free aqueous phase hydrogenation of LA using FA as highly sustainable internal hydrogen source. The influence of various reaction parameters such as like catalyst to substrate ratio, moles of formic acid, time and temperature have studied to achieve highest % conversion. The heterogeneous nature of catalyst was confirmed by hot filtration test. The catalyst was regenerated, reused and the regenerated catalyst was characterized by EDX, FT-

IR, XPS and powder XRD to confirm the sustainability. Also, the catalytic activity of the present catalyst was compared with reported catalysts and the plausible mechanism was also proposed.

EXPERIMENTAL

Materials

All chemicals used were of A.R. grade. Phosphomolybdic acid ($H_3PMo_{12}O_{40}$), palladium chloride ($PdCl_2$), cesium chloride (CsCl), sodium hydrogen carbonate ($NaHCO_3$), levulinic acid and dichloromethane (DCM) obtained from Merck were used as received. Formic acid was acquired from Avra Synthesis Pvt. Ltd.

Synthesis palladium substituted phosphomolybdate

Cesium salt of palladium substituted phosphomolybdate was synthesized by One-pot method as described in chapter 1 (Part A) with some modification. Briefly, a solution of $H_3PM_{12}O_{40}$ (1.825 g, 1 mmol) at pH 4.7, adjusted by adding saturated sodium bicarbonate ($NaHCO_3$), was stirred and heated at 80 °C followed by addition of saturated solution of $PdCl_2$ (0.1773 gm, 1 mmol) and a final pH of 4.7 was also maintained by addition of $NaHCO_3$. The resulting solution was refluxed for 1 h at 80 °C and filtered hot. Then saturated CsCl (0.8418 gm, 5 mmol) solution was added to resulting filtrate. The obtained brown colored precipitates were filtered, washed with water, dried at room temperature and designated as $PMo_{11}Pd(II)$. Finally, brown colored precipitates was charged in a Parr reactor for reduction of Pd(II) to Pd(0), under 1 bar H_2 pressure, at 40 °C for 30 min. The obtained black colored material was designated as $PMo_{11}Pd$. The synthetic scheme is presented in scheme 1.

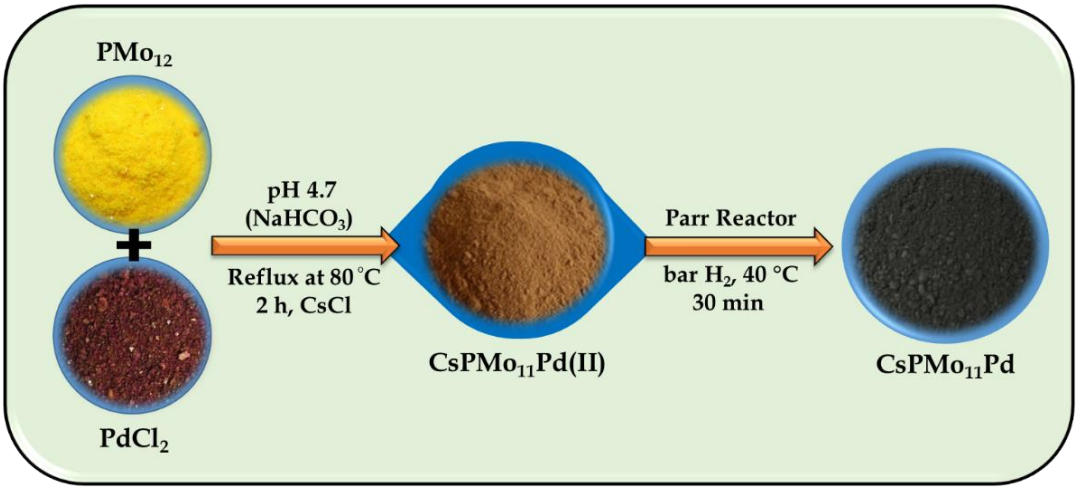

Scheme 1. Synthesis of $PMo_{11}Pd$

Catalytic activity

The hydrogenation of LA to GVL was carried out following the same procedure as mentioned in part B chapter 2.

RESULTS AND DISCUSSION

Please note that, POMs are also act as admirable stabilizing agents due to their fascinating diverse convergent properties such as (i) reducing and encapsulating capacity; which facilitates to the stabilized metal in its most stable oxidation state at significant sites, (ii) robust oxoanionic nature; which significantly improves its stabilization power, (iii) relatively larger sizes; that sterically restricts and inhibits sintering throughout the synthesis as well as during the reaction. Therefore, we have also utilized the advantage of stabilizing property of POMs in the synthesis of $PMo_{11}Pd$ to overcome Pd aggregate formation because it is well known that due to its very high surface energy, they easily undergo aggregate formation during the synthesis or during its utilization. Therefore, the stabilization of Pd nanoparticles is essential.

Characterization

$PMo_{11}Pd$ was isolated by filtration and unreacted molybdenum was analyzed from the filtrate, gravimetrically.[51]. The amount of Mo was found to be 5.1%, equivalent to removal of 1 mmol of Mo from $H_3PMo_{12}O_{40}$.

The EDX of $PMo_{11}Pd$ (Figure 1) shows the presence of all elements (Cs, P, Mo, Pd and O). The found EDX values of the Cs (25.78 wt%), P (1.12 wt%), Mo (40.63 wt%), Pd (4.13 wt%) and O (27.85 wt%) are in good agreement with that of theoretically calculated ones (Cs: 25.66 wt%, P: 1.19 wt%, Mo: 40.75 wt%, Pd: 4.11 wt% and O: 27.80 wt%).

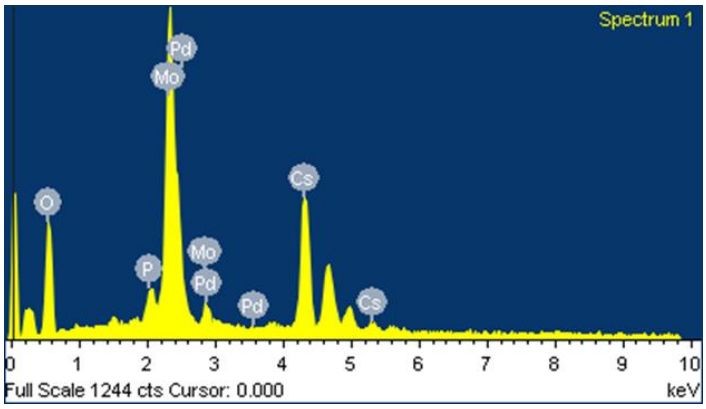

Figure 1. EDX mapping of $PMo_{11}Pd$

TGA of $PMo_{11}Pd$ (Figure 2) gives a weight loss of 5.3% till 100 ^{o}C, corresponding to desorption of physically adsorbed water molecules. It also shows a weight loss of 6.4% in the range of 150 - 320 °C attributed to the presence of crystallization water. After that up to 500 ^{o}C, no substantial weight loss was observed, indicating that the synthesized material is thermally stabile. The number of water molecules was found to be 5, calculated using the formula $18n = \frac{X[M+18n]}{100}$ (n = number of water molecules, X = percentage loss from TGA, and M= the molecular weight of the catalyst). Based on the above study, the composition of the synthesized catalyst is proposed as $Cs_5[PMo_{11}O_{39}Pd(H_2O)].5H_2O$.

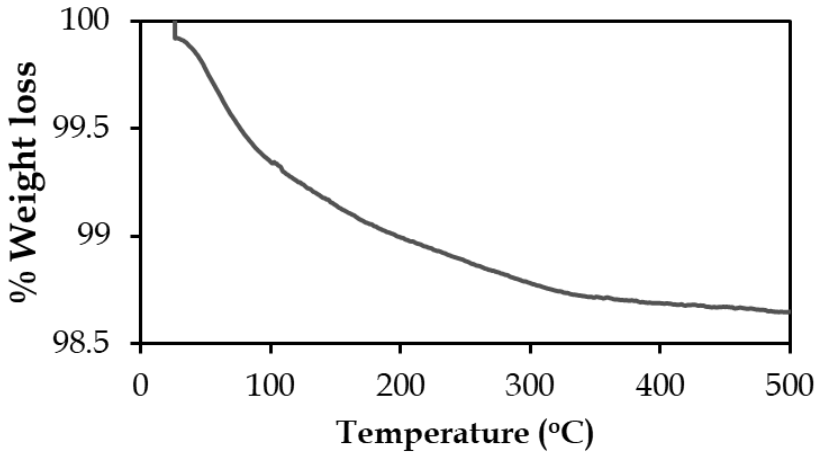

Figure 2. TGA of $PMo_{11}Pd$

The FT-IR spectra of PMo_{12}, PMo_{11} and $PMo_{11}Pd$ are displayed in the Figure 3. PMo_{12} shows (Figure 3a) characteristic bands at 1060, 965, 870 and 790 cm^{-1} which corresponds to ν_s P-O_a, ν_{as} Mo=O_t and ν_{as} Mo-O_b-Mo and ν_{as} Mo-O_c-Mo stretching vibration respectively [52]. Whereas, PMo_{11} shows (Figure 3b) all characteristic bands of PMo_{12} at 1064 and 1045 cm^{-1} corresponding to ν_{as} P-O_a stretching, at 964 cm^{-1} corresponding to ν_{as} Mo=O_t stretching, at 871 cm^{-1} corresponding to ν_{as} Mo-O_b-Mo stretching and at 791 corresponding to ν_{as} Mo-O_c-Mo stretching vibrations respectively [52, 53]. The FT-IR spectrum of $PMo_{11}Pd$ also shows (Figure 3c) splitting in P-O stretching band similar to PMo_{11} with significant shifting towards lower frequency at 1042 and 1012 cm^{-1}, which clearly indicates that Pd was introduced in to the octahedral lacuna. Similarly, it also shows other characteristic bands of Keggin unit with significant shifting at 939 cm^{-1} (Mo=O), and 731 cm^{-1} (Mo-O_c-Mo) respectively.

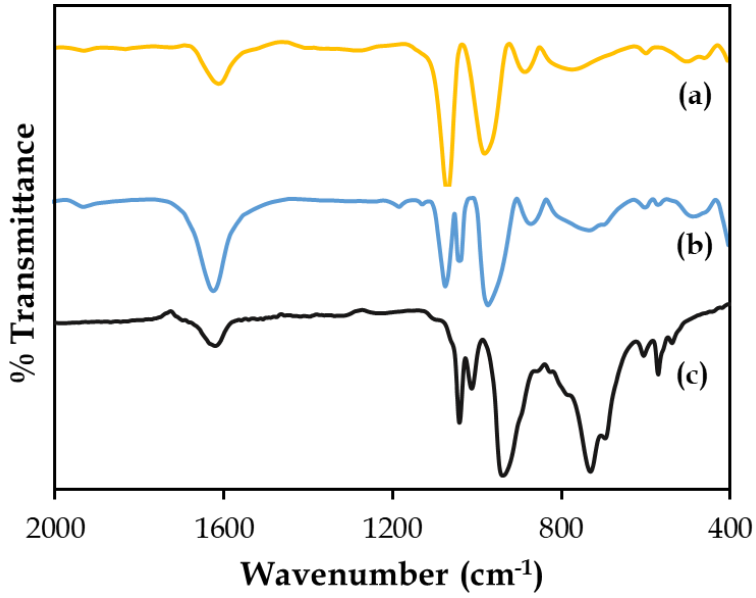

Figure 3. FT-IR spectra of (a) PMo_{12}, (b) PMo_{11} and (c) $PMo_{11}Pd$

^{31}P MAS NMR of PMo_{12} and $PMo_{11}Pd$ were recorded to study the chemical environment surrounding the phosphorus after insertion of Pd into PMo_{11} lacuna. ^{31}P MAS NMR of PMo_{12} shows (Figure 4a) high intensity peak at -3.815 ppm which is identical with reported one [52]. Whereas ^{31}P MAS NMR of $PMo_{11}Pd$ shows (Figure 4b) intense peak with significant downfield shifting from -3.815 to 7.797 ppm [36]. The obtained downfield shifting in NMR peak indicates that the palladium is inserted into lacuna to generate lower symmetry around central hetero atom phosphorus with retention of Keggin unit.

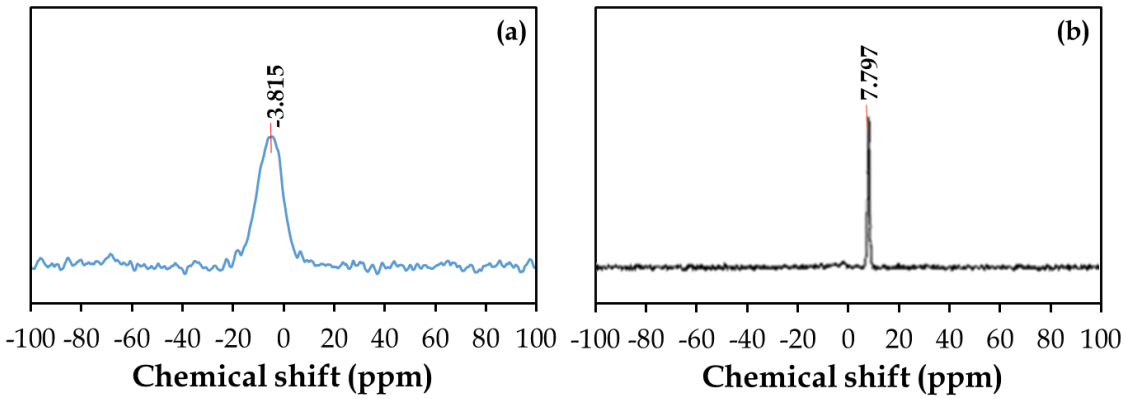

Figure 4. ^{31}P MAS NMR of (a) PMo_{12} and (b) $PMo_{11}Pd$

Figure 5a shows full range XPS of $PMo_{11}Pd$ was performed (Figure 5) to elucidate the oxidation states of Cs, Pd, O and Mo.. Figure 5b displays two peaks at 334.78 and 340.9 eV corresponding to spin-orbits $3d_{5/2}$ and $3d_{3/2}$ respectively which confirms that Pd is present in metallic state (Pd^0) [34-36]. Similarly, two doublet intense energy peaks i) at 233 and 235 eV corresponding to $3d_{5/2}$ and $3d_{3/2}$ energy levels of 3d orbital (Figure 5c) respectively and ii) at 397, and 416 eV corresponding to $3p_{3/2}$ and $3p_{1/2}$ energy levels of 3p orbital respectively attributed to Mo^{6+} [54, 55], confirming that Mo is not reduced during reduction of Pd(II) to Pd(0). Also, it shows a highly intense binding energy peak at 532 eV attributed to oxygen (O1s) present in PMo_{11}. Two additional high intense energy peaks obtained at 741 and 724 eV are attributed to $Cs3d_{5/2}$ and $Cs3d_{5/2}$, respectively [56, 57].

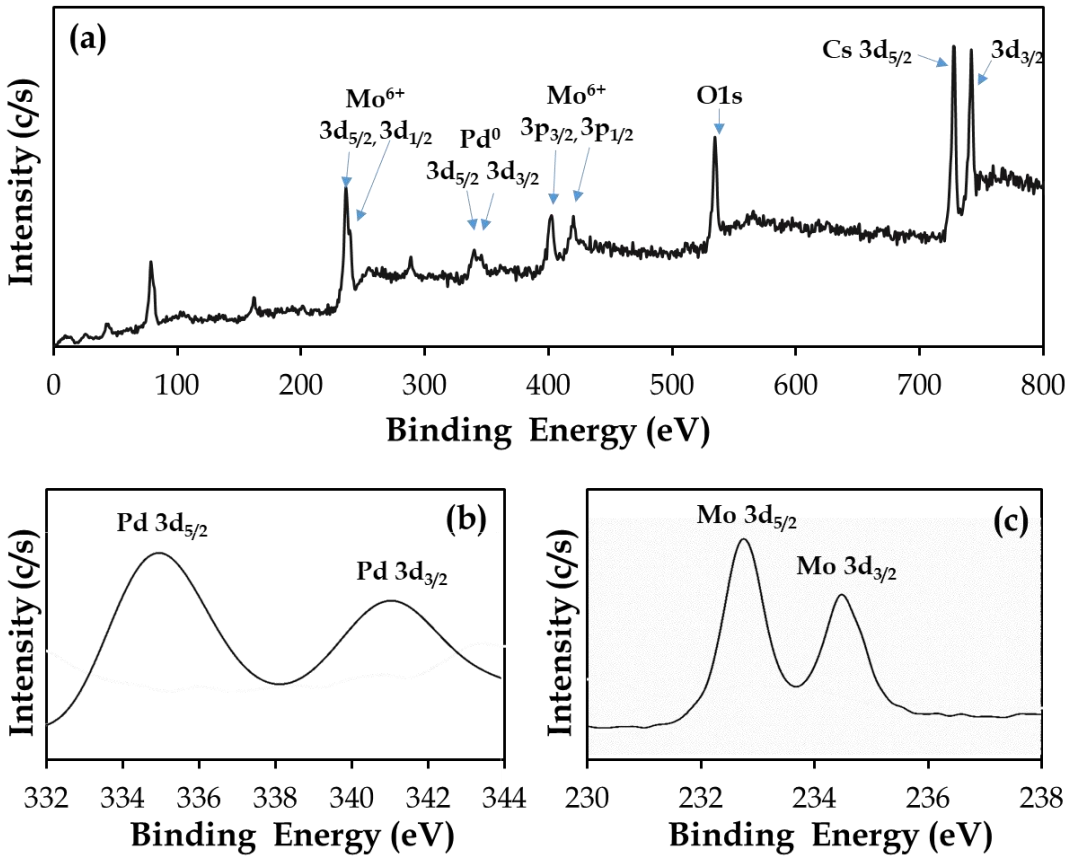

Figure 5. XPS spectra of $PMo_{11}Pd$

The Powder XRD patterns of PMo_{12} and $PMo_{11}Pd$ are presented in Figure 6. The characteristic 2θ peaks in the range of 15° to 35° are accredited to Keggin unit of PMo_{12} [52]. A distinct shift in 2θ value of PMo_{11} (Figure 6b) from 25-35° is observed due to the formation of lacuna by removing one Mo=O unit. Similarly, the powder XRD pattern of $PMo_{11}Pd$ shows (Figure 6c) all characteristic peaks of PMo_{12} with slight shift in peaks at 18.34°, 25.25°, 26.98° and 30.05° due to Pd incorporation in PMo_{11} with retention of Keggin structure [35, 36]. Also shown additional small peaks at 41.81° and 45.96° correspond to Pd(111) and Pd(200) crystallographic plane, which is in good agreement with reported one [36].

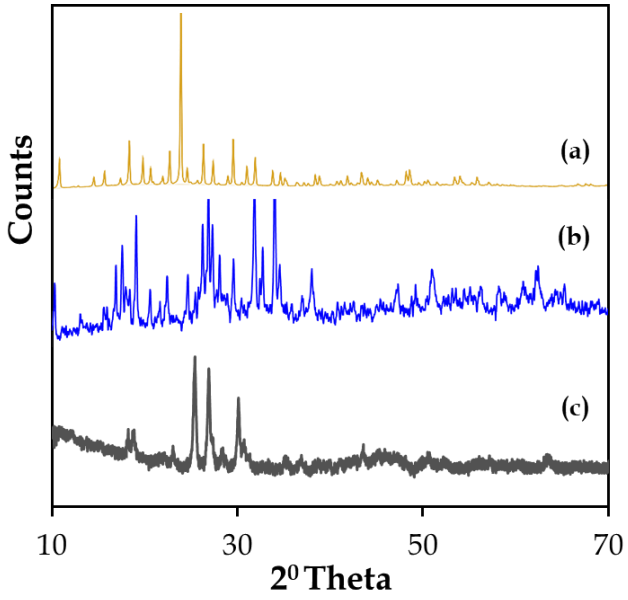

Figure 6. Powder XRD of (a) PMo_{12} (b) PMo_{11} and (c) $PMo_{11}Pd$

TEM images of $PMo_{11}Pd$ were taken at various resolutions. Figure 7a-b shows the presence of very small, dispersed Pd nanoparticles. High-resolution image of TEM (Figure 7c) shows spherical morphology of $PMo_{11}Pd$ with uniform homogeneous dispersion at 20 nm, indicating that Pd NPs are stabilized into lacuna of PMo_{11}. To confirm this HR-TEM of $PMo_{11}Pd$ were recorded. It is clearly observed (Figure 7d-f) that isolated Pd NPs with <5 nm size is uniformly dispersed throughout the morphology.

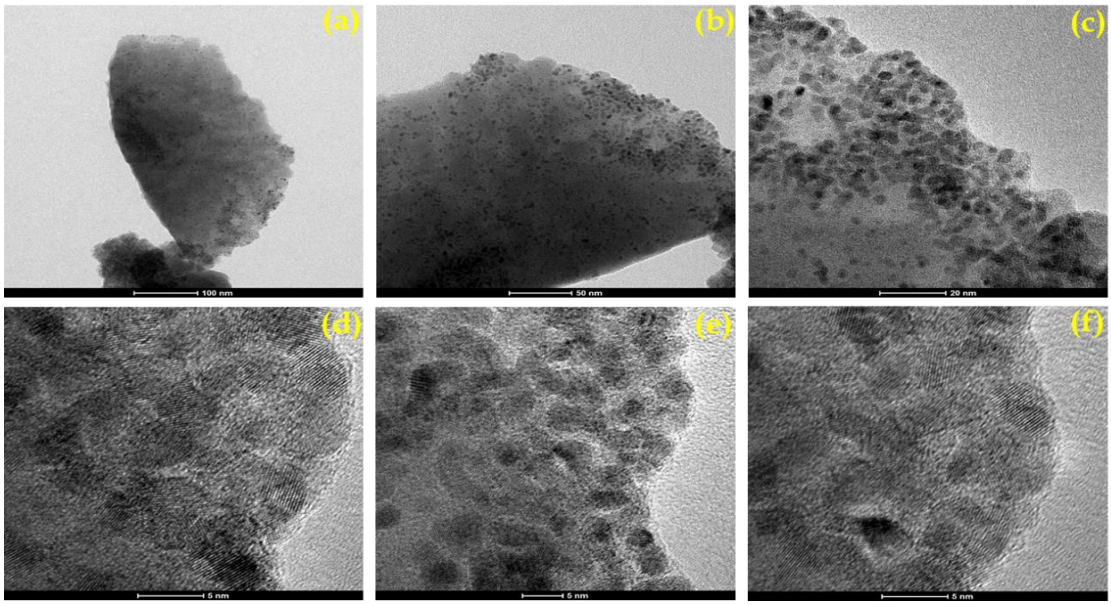

Figure 7. (a-c) TEM and (d-f) HRTEM of $PMo_{11}Pd$

To confirm presence of isolated Pd NPs HAADF-STEM EDX analysis was also carried out. The bright filed and dark field images show (Figure 8a) the presence of isolated Pd NPs with uniform dispersion. The STEM-EDX mapping image of Pd (Figure 8e) and overlapping images (Figure 8g) clearly shows isolated Pd NPs without any aggregation between them. STEM-EDX images shows presence of all element in the synthesized $PMo_{11}Pd$.

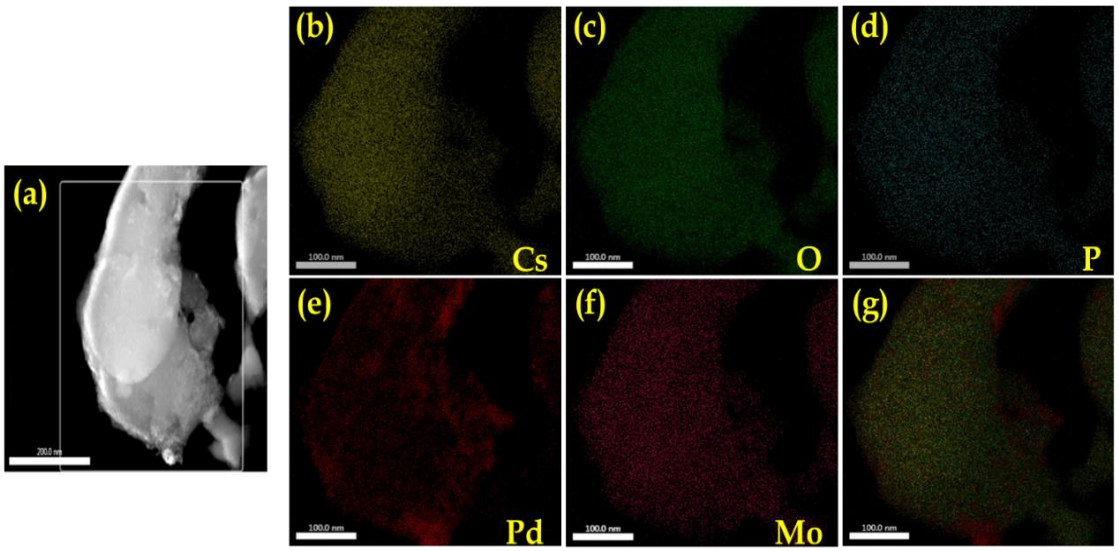

Figure 8. (a) HAADF-STEM and (b-g) EDX images of $PMo_{11}Pd$

In the summary, FT-IR and ^{31}P MAS NMR shows the insertion of palladium in to lacuna (PMo_{11}) with retention of Keggin unit. XPS and TEM confirms the present of Pd (0) and Mo (VI) while HR-TEM and STEM-EDX reveals uniform dispersion of Pd NPs.

Catalytic activity

The synthesized catalyst, $PMo_{11}Pd$ was explored for liquid phase hydrogenation of LA using FA as a sustainable hydrogen source. To effect of various parameters such as amount of catalyst, mole ratio of LA to FA, reaction time as well as temperature were studied to achieve maximum conversion.

Figure 9a shows an effect of catalyst varying catalyst amount from 50-5 mg, where all other parameters kept constant. It is observed from the data that a % conversion (99%) remains same for 50 and 25 mg of catalyst while decreased for 20 and 15mg. However, on decreasing the catalyst amount further to 10 and 5 mg, there was decrease in % conversion to 92 and 86% respectively. Therefore, 20 mg of catalyst was enough to achieve maximum % conversion using 125mmol of FA. However, we thought that used amount of FA (125 mmol) is very high, therefore we have selected 5 mg catalyst (minimum amount) to study its effect on different amounts of formic acid for achieve maximum conversion.

The influence of FA was studied by varying amount FA from 125 to 5 mmol and obtained results are depicted in Figure 9b. The obtained results suggest that with decreasing amount of FA from 125 to 5 mmol, there is increase in the % conversion (from 87 to 95% respectively) of LA which may be due to the reactant (LA) and hydride which gets easily adsorb on active catalyst site for the catalytic transformation. Based on this study, 5 mmol of FA was selected to obtained highest conversion (95%) and used for further optimization studies.

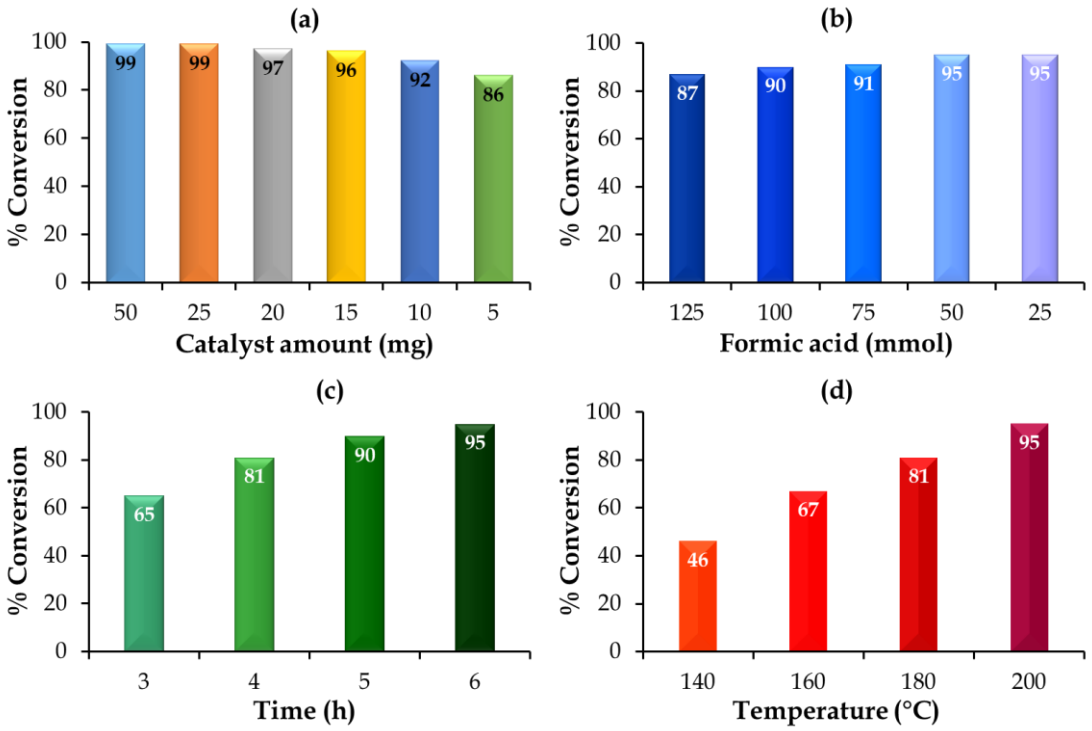

Figure 9. Optimization of reaction parameters for LA hydrogenation. Reaction conditions: (a) Effect of catalyst amount- LA (5 mmol), FA (125 mmol), time (6 h) and temperature (200 °C); (b) Effect of Formic acid- catalyst (5 mg Pd), LA (5 mmol), time (6 h) and temperature (200 °C); (c) Effect of time- catalyst (5 mg), LA (5 mmol), FA (25 mmol) and temperature (200 °C); (d) Effect of temperature- catalyst (5 mg), LA (5 mmol), FA (25 mmol) and time (6 h).

Effect of reaction time (Figure 9c) shows that % conversion increases gradually from 65% to 95% with increase in time from 3 h to 6 h respectively. As it is well-known fact that with increase in time, there is increase in the conversion of reactant to reactive intermediates which further transforms into product. Therefore, the obtained result is in good agreement and hance 6 h time was optimized to get 95% conversion.

Finally, the effect of reaction temperature was also screened from 140 and 200 °C with an interval of 20 °C to achieve maximum conversion. The obtained result (Figure 9d) shows that %conversion increased with increase in temperature up to 200 °C. This may be due to with increase in temperature, the rate of FA decomposition is increased to produce maximum amount of hydrogen which

transforms more LA to produce GVL. Thus, 200 °C temperature was optimized to obtain highest 95% conversion.

Based on this study optimized conditions for maximum 95% conversion are: Catalyst (5 mg), active amount of Pd ($1.879*10^{-3}$ mmol), LA (5 mmol), substrate/catalyst ratio (2661), FA (25 mmol), time (6 h), temperature (200 °C) and TON (2528).

The gas chromatograph of optimized reaction condition for LA hydrogenation is shown in figure 10.

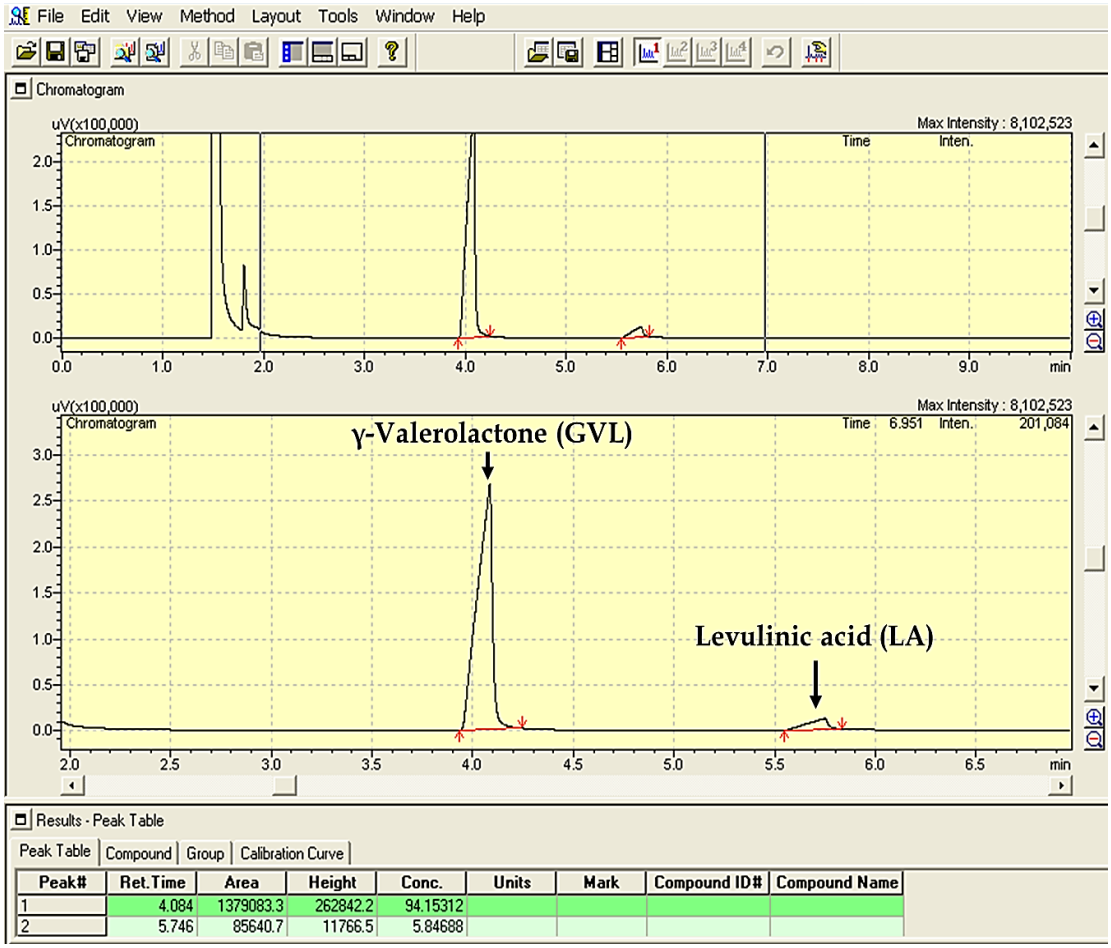

Figure 10. Gas chromatograph of levulinic acid hydrogenation

Control experiment

In order to study the role of all components, control experiments were performed under optimized condition (table 1) without FA, without catalyst,

PMo_{11} and $PdCl_2$. From table 1, it is seen that under identical reaction conditions, 0% conversion was obtained for entry number 1-3 indicating that both catalyst and FA are important for reaction progression. Also, it shows PMo_{11} is totally inactive towards the reaction. However, $PdCl_2$ and $PMo_{11}Pd$ were given almost same conversion (90% and 95% respectively).

Since $PdCl_2$ is easily soluble in the reaction mixture due to its homogeneous nature and it also results in the formation of aggregates. Therefore, it becomes difficult to recover and recycle it after completion of the reaction. However, when the reaction is carried out using $PMo_{11}Pd$, it is insoluble in the reaction mass and hence it is heterogeneous in nature. Therefore, it can be easily recovered as well as recycled. Also, PMo_{11} stabilizes Pd NPs by resisting formation of the aggregates during the reaction.

Table 1. Control experiment

Catalyst	% Conversion
Without H_2	-
Without catalyst	-
[a]PMo_{11}	-
[b]$PdCl_2$	90
$PMo_{11}Pd$	95

Reaction conditions: Catalyst ([a]4.8 mg, [b]4.8 mg, 5 mg, Pd: $1.879*10^{-3}$ mmol), LA (5 mmol), FA (25 mmol), time (6 h) and temperature (200 °C).

Hot filtration and heterogeneity test

In heterogeneous catalysis, the catalyst should preserve its heterogeneity while retaining its active sites unchanged over many cycles is one of the most fundamental necessities. To affirm this, a hot filtration experiment was carried out to explore the leaching of Pd from the lacuna of PMo_{11} under optimized reaction conditions. The reaction was initiated with $PMo_{11}Pd$ and proceeded for 3 hours. The catalyst was then removed using simple centrifugation, and the reaction was continued for another 6 hours with the filtrate (another 3h). After

the reaction was accomplished, the organic layer was separated using dichloromethane and then it was analyzed with a gas chromatogram. Obtained almost same % conversion confirming that no leaching of Pd from catalyst during the reaction (Table 2). Moreover, it demonstrates that PMo11 stabilizes Pd throughout the reaction and makes the process truly heterogeneous, reflected in the recycling study.

Table 2. Hot filtration test

Catalyst	% Conversion
$PMo_{11}Pd$	44 (after 3 hour)
	45 (after 6 hour)

Reaction conditions: Catalyst (5 mg), LA (5 mmol), FA (25 mmol), time (6 h) and temperature (200 °C).

Regeneration and recycling studies

For any catalytic process, the catalyst sustainability is a key issue. As described in Part A and B, after completion of the reaction, the catalyst was centrifuged and washed with dichloromethane, water as well as finally air dried and charged for the next catalytic cycle (Table 3). No appreciable change in % conversion up to three catalytic runs clearly shows that catalyst is sustainable and truly heterogeneous in nature.

Table 3. Recycling studies

Catalyst	% Conversion
$PMo_{11}Pd$	95
Recycle – 1	95
Recycle – 2	94
Recycle – 3	94

Reaction conditions: Catalyst (5 mg), LA (5 mmol), FA (25 mmol), time (6 h) and temperature (200 °C).

Characterization of regenerated catalyst

The regenerated catalyst was characterized by various physicochemical techniques such as EDX, FT-IR, XPS and powder XRD analysis to confirm the retention of catalyst structure.

The found EDX values of Cs (25.88 wt%), P (1.14 wt %), Mo (40.53 wt%), Pd (4.12 wt %) and O (28.92 wt%) for regenerated $PMo_{11}Pd$ are in good agreement with the fresh one, which confirms that there was no leaching of Pd as well as Mo from the lacuna during the reaction. Also, elemental mapping shows (Figure 11) presence of all elements.

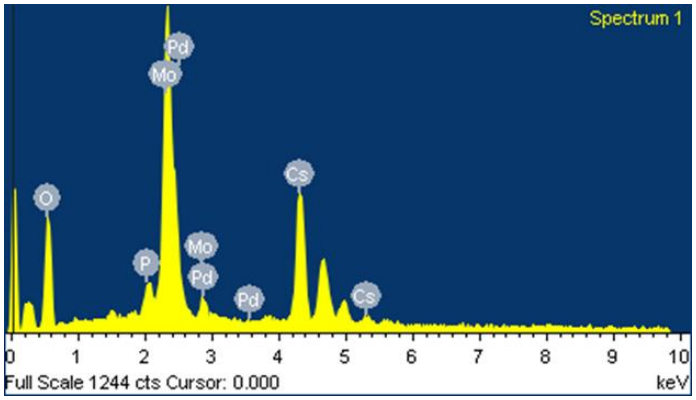

Figure 11. EDX analysis of regenerated $PMo_{11}Pd$

Figure 11b depicts the FT-IR of the regenerated $PMo_{11}Pd$ is identical with fresh $PMo_{11}Pd$ (Figure 11a) which demonstrate that the catalyst structure remains intact even after regeneration. In comparison to the fresh catalyst, the regenerated catalyst displays bands with slightly reduced intensity which can be due to sticking of substrates to the catalyst.

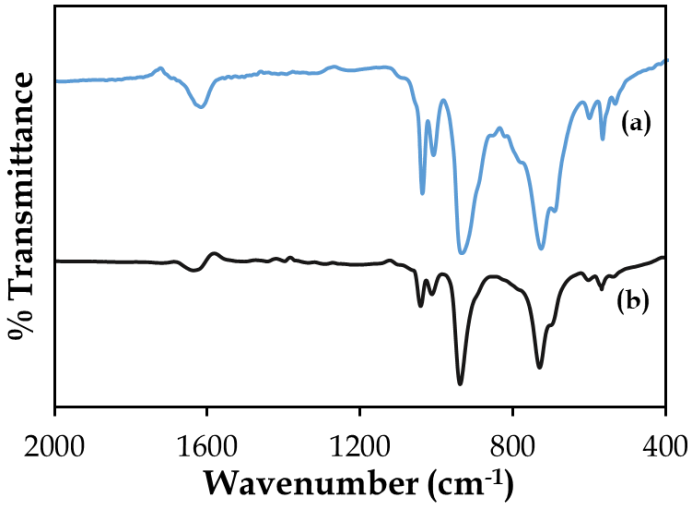

Figure 12. FT-IR spectra of (a) fresh $PMo_{11}Pd$ and (b) regenerated $PMo_{11}Pd$

The XPS analysis of regenerated $PMo_{11}Pd$ (Figure 13) reveals that all the characteristic binding energy peaks of Cs, Mo, Pd and O are identical to those found in the fresh catalyst (Figure 5). It further confirms that Mo (VI) does not get reduced during the reaction.

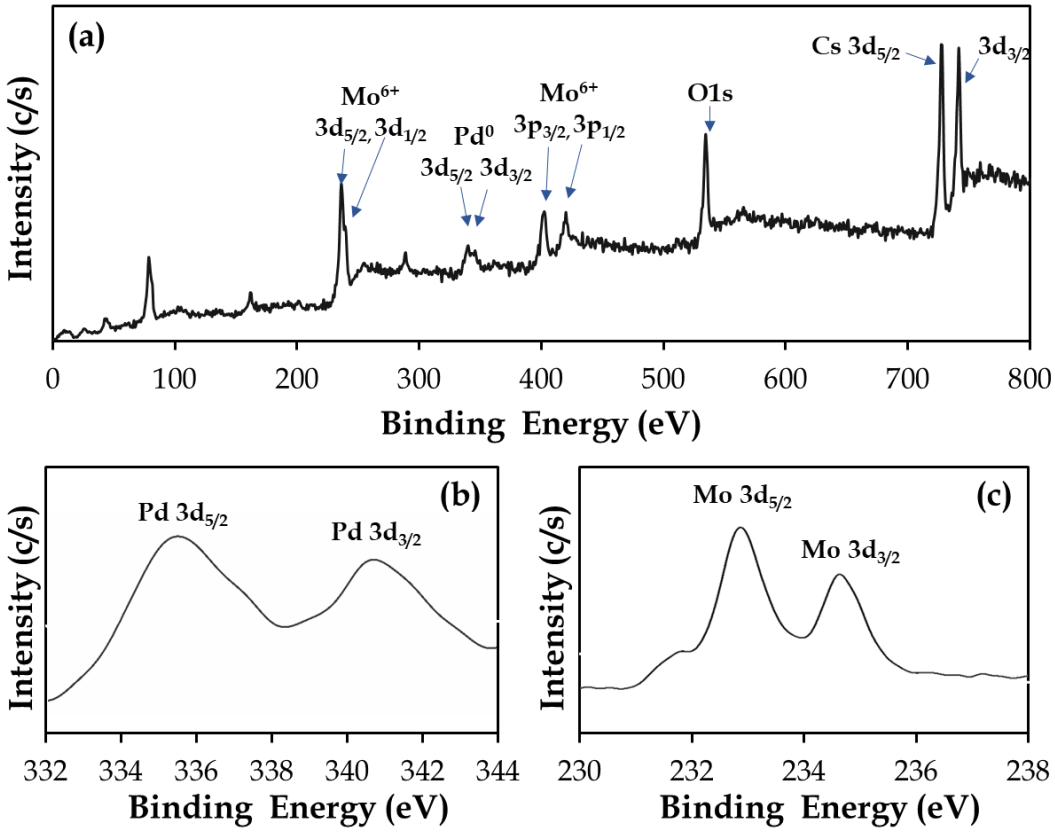

Figure 13. XPS of regenerated $PMo_{11}Pd$

XRD pattern of regenerated $PMo_{11}Pd$ and $PMo_{11}Pd$ are displayed in figure 14. The XRD spectra of regenerated $PMo_{11}Pd$ is undistinguishable with $PMo_{11}Pd$ with retention of characteristic peaks of Pd NPs which clearly indicates the sustainability of the catalyst during the reaction.

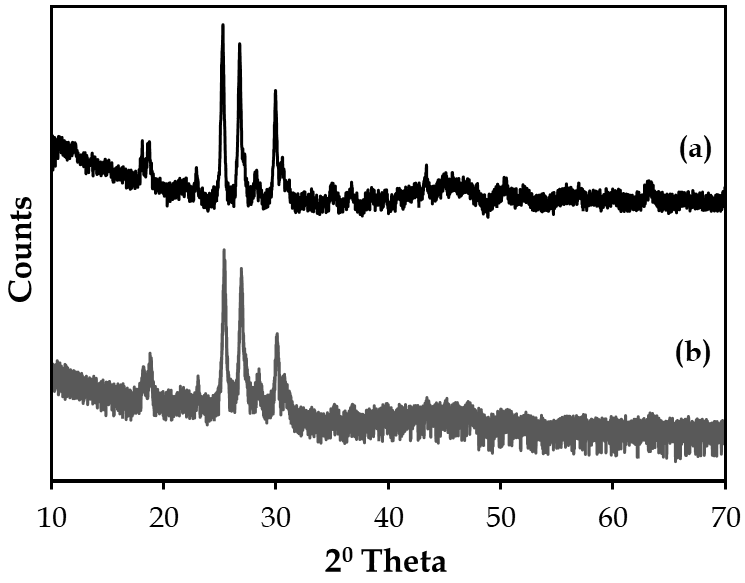

Figure 14. Powder XRD paten of (a) fresh $PMo_{11}Pd$ and (b) regenerated $PMo_{11}Pd$

Mechanistic investigation

For LA to GVL transformation over $PMo_{11}Pd$, we are expecting the same mechanism as explained in part B chapter 2 for Ni-PMO_{12}/ZrO_2. Hence, detailed explanation is not included here but mechanism pathway shown in scheme 2.

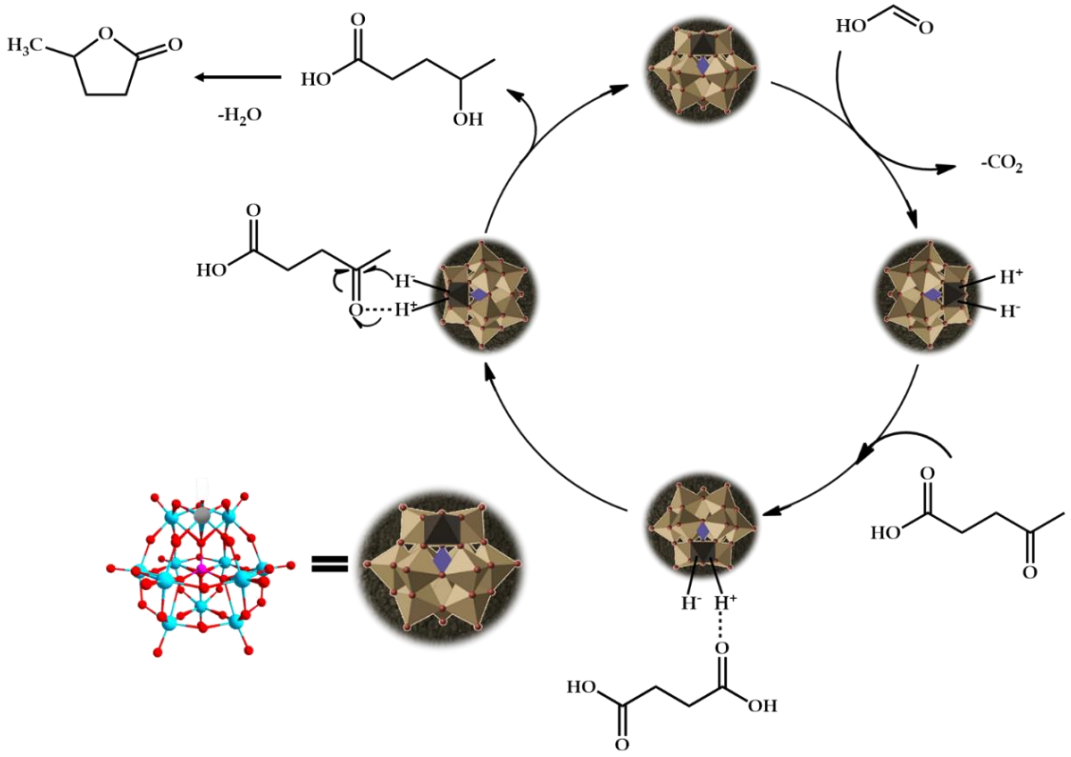

Scheme 2. Plausible reaction mechanism for LA hydrogenation reaction

Comparison with reported catalyst

The catalytic activity of $PMo_{11}Pd$ is compared with reported catalyst as shown in Table 4. It is seen that harsh, entry 1-7, different Pd based catalyst reaction conditions (high catalyst quantity, solvent, time, and temperature). Moreover, they require high pressure of H_2 which becomes difficult to handle. However, when FA is used (as a hydrogen source), high amount of Pd (wt%), time and temperature are required to get 93% and 95% conversion respectively (Entry 8and 9). In this regard, the present catalyst superior as compared to previously reported catalysts in terms of catalyst amount, H source, reaction time, and temperature under solvent-free conditions.

Table 4. Comparison with reported catalyst

Sr. No.	Catalyst	Catalyst (Wt%)	LA (mmol)	H- source (mL/ bar)	Solvent	Time (h)	Temp. (°C)	% Conversion
1	Pd/CeO_2 [44]	0.873	0.175	H_2 (4 bar)	2-PrOH (5 mL)	0.1	100	33
2	[(dtbpe)Pd Cl_2][42]	0.1	0.0033	H_2 (5 bar)	H_2O (15 mL)	5	80	100
3	Pd/MCM-41[40]	5	25	H_2 (40 bar)	H_2O (5mL)	10	240	99
4	Pd/ND [46]	0.1	0.0045	H_2 (7 bar)	-	12	150	96
5	2PdZSM5 [47]	10	17.22	H_2 (40 bar)	EtOH (15 mL)	8	240	92
6	$Pd@m_{16}SiO_2$ [50]	0.01	3.1	H_2 (30 bar)	Dioxane (6 mL)	3	200	96
7	Pd@UiO-66-NH_2 [49]	0.94	5	H_2 (20 bar)	H_2O	2	140	98
8	Pd-Fe_3O_4/PPTPA-1 [45]	0.42	1	FA (1 mL)	EtOH (2mL)	12	140	93
9	m-SiO_2@Pd@SiO_2 [43]	0.616	1	FA (1 mL)	H_2O (5 mL)	15	120	95
10	**$PMo_{11}Pd$**	**0.205**	**5**	**FA (1 mL)**	**-**	**6**	**200**	**95**

CONCLUSION

- **$Cs_5[PMo_{11}O_{39}Pd(H_2O)].5H_2O$** was designed by **One-Pot method** and characterized by **various physicochemical techniques** to confirm the **incorporation** of **Pd** into **lacuna** with retention of Keggin unit.
- The catalyst exhibited the **high activity** (**95%** conversion) towards **hydrogenation** of **LA using FA** as **an internal hydrogen** source under **solvent free** condition.
- The **true heterogeneous nature** of the catalyst was revealed by **hot filtration** test.
- The catalyst is **regenerated** and reused up to **three catalytic cycles** (and can be used for more) **without decay in activity**. The **retention** of the **catalyst structure** was further confirmed through the characterization of the regenerated catalyst by EDX, FT-IR, XPS and Powder XRD.

REFERENCES

[1] A. Patel, N. Narkhede, S. Singh, S. Pathan, Catal. Rev., 58, 337, (2016).

[2] J. W. Zhao, Y.-Z. Li, L.-J. Chen, G.-Y. Yang, Chem. Commun., 52, 4418, (2016).

[3] V. Das, R. Kaushik, F. Hussain, Coord. Chem. Rev., 413, 213271, (2020).

[4] A. Patel, R. Sadasivan, Prog. Mater. Sci., 118, 100759, (2021).

[5] P. Putaj, F. Lefebvre, Coord. Chem. Rev., 255, 1642, (2011).

[6] N. V. Izarova, M. T. Pope, U. Kortz, Angew. Chem. Int. Ed., 51, 9492, (2012).

[7] R. Neumann, C. Abu-Gnim, J. Am. Chem. Soc., 112, 6025, (1990).

[8] C. Rong, M. T. Pope, J. Am. Chem. Soc., 114, 2932, (1992).

[9] R. Neumann, M. Dahan, Polyhedron, 17, 3557, (1998).

[10] L. Xinrong, X. Jinyu, L. Huizhang, Y. Bin, J. Songlin, X. Gaoyang, J. Mol. Catal. A: Chem., 161, 163, (2000).

[11] M. Sadakane, D. Tsukuma, M. H. Dickman, B. Bassil, U. Kortz, M. Higashijima, W. Ueda, Dalton Trans., 4271, (2006).

[12] P. Shringarpure, A. Patel, Inorganica Chim. Acta, 362, 3796, (2009).

[13] C. G. Liu, W. Guan, L. K. Yan, Z. M. Su, Eur. J. Inorg. Chem., 2011, 489, (2011).

[14] A. M. Khenkin, I. Efremenko, L. Weiner, J. M. L. Martin, R. Neumann, Chem. Eur. J., 16, 1356, (2010).

[15] B. Zhu, Z. L. Lang, N. N. Ma, L. K. Yan, Z. M. Su, Phys. Chem. Chem. Phys., 16, 18017, (2014).

[16] M. Bonchio, M. Carraro, A. Sartorel, G. Scorrano, U. Kortz, J. Mol. Catal. A: Chem., 251, 93, (2006).

[17] K. Ikeda, K. Yoshizawa, Y. Shiota, Inorganic Chemistry, 61, 10, (2022).

[18] Y. Matsumoto, M. Asami, M. Hashimoto, M. Misono, J. Mol. Catal. A: Chem., 114, 161, (1996).

[19] X. Wei, M. H. Dickman, M. T. Pope, Inorg. Chem., 36, 130, (1997).

[20] X. Wei, R. E. Bachman, M. T. Pope, J. Am. Chem. Soc., 120, 10248, (1998).

[21] K. M. Wiaderek, J. A. Cox, Electrochim. Acta, 56, 3537, (2011).

[22] M. N. Sokolov, S. A. Adonin, P. L. Sinkevich, C. Vicent, D. A. Mainichev, V. P. Fedin, Z. fur Anorg. Allg. Chem., 640, 122, (2014).

[23] D. Laurencin, R. Villanneau, H. Gérard, A. Proust, J. Phys. Chem. A, 110, 6345, (2006).

[24] C. Dablemont, C. G. Hamaker, R. Thouvenot, Z. Sojka, M. Che, E. A. Maatta, A. Proust, Chem. Eur. J., 12, 9150, (2006).

[25] D. Pan, J. Chen, W. Tao, L. Nie, S. Yao, Langmuir, 22, 5872, (2006).

[26] M. H. Seo, S. M. Choi, H. J. Kim, J. H. Kim, B. K. Cho, W. B. Kim, J. Power Sources, 179, 81, (2008).

[27] H. Li, X. Zhang, H. Pang, C. Huang, J. Chen, J. Solid State Electrochem., 14, 2267, (2010).

[28] Z. Cui, W. Xing, C. Liu, D. Tian, H. Zhang, J. Power Sources, 195, 1619, (2010).

[29] S. Li, X. Yu, G. Zhang, Y. Ma, J. Yao, P. de Oliveira, Carbon, 49, 1906, (2011).

[30] Z. Cui, C. M. Li, S. P. Jiang, Phys. Chem. Chem. Phys., 13, 16349, (2011).

[31] X. Jin, B. He, J. Miao, J. yuan, Q. Zhang, L. Niu, Carbon, 50, 3083, (2012).

[32] Z. Bai, C. Zhou, N. Gao, H. Pang, H. Ma, RSC Adv., 6, 937, (2016).

[33] F. Amouzad, K. Zarei, J. Electron. Mater., 49, 3583, (2020).

[34] V. Kogan, Z. Aizenshtat, R. Popovitz-Biro, R. Neumann, Org. Lett., 4, 3529, (2002).

[35] V. Kogan, Z. Aizenshtat, R. Neumann, New J. Chem., 26, 272, (2002).

[36] S. Rana, K. M. Parida, Catal. Sci. Technol., 2, 979, (2012).

[37] M. J. Hülsey, V. Fung, X. Hou, J. Wu, N. Yan, Angewandte Chemie International Edition, 61, e202208237, (2022).

[38] S. H. Gebre, Appl. Nanosci., (2021).

[39] M. Aksoy, H. Kilic, B. Nişancı, Ö. Metin, Inorg. Chem. Front., 8, 499, (2021).

[40] K. Yan, T. Lafleur, C. Jarvis, G. Wu, J. Clean. Prod., 72, 230, (2014).

[41] A. S. Amarasekara, M. A. Hasan, Catal. Commun., 60, 5, (2015).

[42] C. Ortiz-Cervantes, M. Flores-Alamo, J. J. García, ACS Catal., 5, 1424, (2015).

[43] B. Banerjee, R. Singuru, S. K. Kundu, K. Dhanalaxmi, L. Bai, Y. Zhao, B. M. Reddy, A. Bhaumik, J. Mondal, Catal. Sci. Technol., 6, 5102, (2016).

[44] Y. Zhang, C. Chen, W. Gong, J. Song, H. Zhang, Y. Zhang, G. Wang, H. Zhao, Catal. Commun., 93, 10, (2017).

[45] K. Dhanalaxmi, R. Singuru, S. Mondal, L. Bai, B. M. Reddy, A. Bhaumik, J. Mondal, ACS Sustain. Chem. Eng., 5, 1033, (2017).

[46] N. Gupta, N. Dimitratos, D. Su, A. Villa, Energy Technol., 7, 269, (2019).

[47] M. Muñoz-Olasagasti, A. Sañudo-Mena, J. A. Cecilia, M. L. Granados, P. Maireles-Torres, R. Mariscal, Top. Catal., 62, 579, (2019).

[48] C. Y. Hsiao, H. Y. Chiu, T. Y. Lin, K. Y. A. Lin, Chem. Eng. Commun., 208, 1511, (2021).

[49] J. Feng, M. Li, Y. Zhong, Y. Xu, X. Meng, Z. Zhao, C. Feng, Microporous Mesoporous Mater., 294, 109858, (2020).

[50] Y. Liu, Q. Xin, D. Yin, S. Liu, L. Li, C. Xie, S. Yu, Catal. Lett., 150, 3437, (2020).

[51] A. I. Vogel, G. H. Jeffery, Vogel's Textbook of Quantitative Chemical Analysis, Longman Scientific & Technical, (1989).

[52] N. Mizuno, J. S. Min, A. Taguchi, Chem. Mater., 16, 2819, (2004).

[53] M. Rabbani, Z. S. Seghatoleslami, R. Rahimi, J. Mol. Struct., 1146, 113, (2017).

[54] C. Wan, B. M. Leonard, Chem. Mater., 27, 4281, (2015).

[55] D. Yu, W. Gao, S. Xing, L. Lian, H. Zhang, X. Wang, D. lou, RSC Adv., 9, 4884, (2019).

[56] A. Patel, A. Patel, Catal. Lett., 151, 803, (2021).

[57] W. T. Liu, S. C. Tsai, T. L. Tsai, C. P. Lee, C. H. Lee, J. Radioanal. Nucl. Chem., 314, 2237, (2017).

CHAPTER 2

Palladium exchanged phosphomolybdic acid supported on zirconia ($Pd\text{-}PMo_{12}/ZrO_2$): Synthesis, characterization and application for Tandem Suzuki–Miyaura cross coupling/ nitro hydrogenation

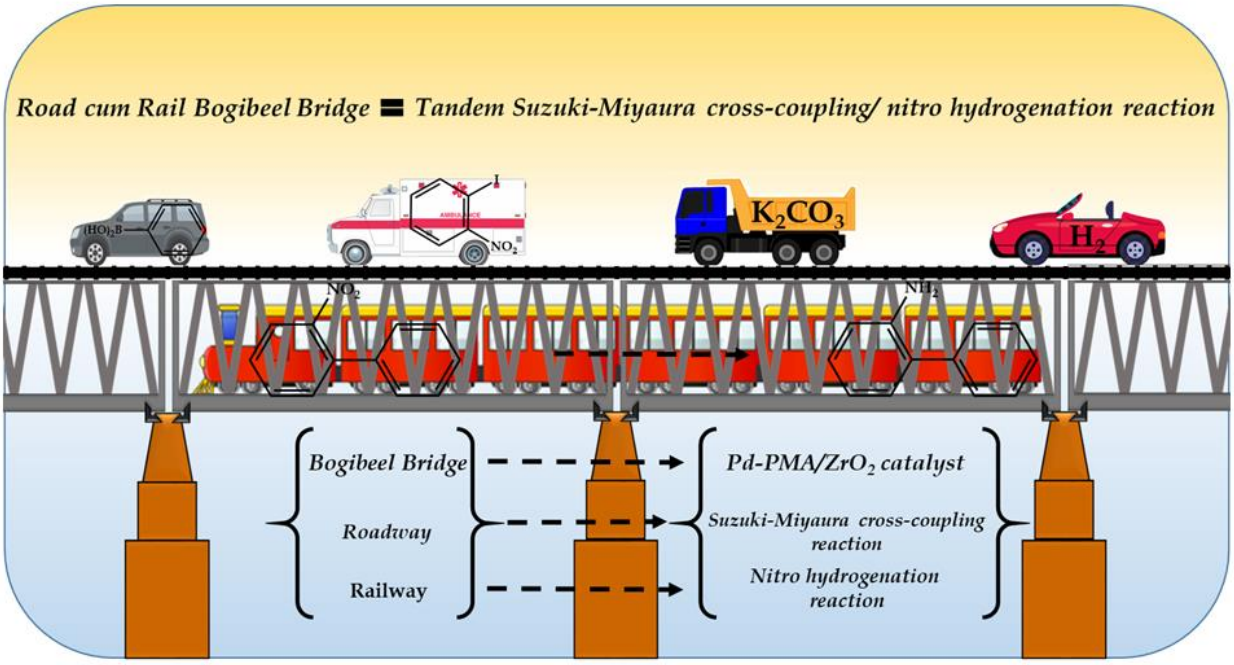

Nanoscale Advances

ROYAL SOCIETY OF CHEMISTRY

PAPER

View Article Online
View Journal

Cite this: DOI: 10.1039/d2na00559j

Pd single-atom-site stabilized by supported phosphomolybdic acid: design, characterizations and tandem Suzuki–Miyaura cross coupling/nitro hydrogenation reaction†

Jay R. Patel and Anjali U. Patel *

Received 22nd August 2022
Accepted 5th September 2022

DOI: 10.1039/d2na00559j

rsc.li/nanoscale-advances

Herein, a single-metal (Pd) site with high surface energy was stabilized and dispersed on a support (zirconia) *via* a stabilizing agent (phosphomolybdic acid) using a wet chemistry method. HRTEM and HAADF-STEM showed a highly uniform dispersion of Pd SASc on PMA/ZrO_2. The Pd SASc showed superior catalytic activity (>99% conversion) for the Suzuki–Miyaura cross-coupling reaction, which was further feasible for catalyzing mechanistically different nitro hydrogenation reactions in tandem fusion under mild reaction conditions. This catalyst showed outstanding activity (100% conversion and 99% selectivity) with a substrate/catalyst ratio of 927 and TON of 918 using a very low amount of Pd (0.94×10^{-3} mmol) for the tandem Suzuki–Miyaura cross-coupling/nitro hydrogenation reaction. It also exhibited superior stability and reusability for up to three cycles without any change in its activity.

* Published with full waving

As mentioned in general introduction, supported phosphomolybdic acid (PMo_{12}) have been used as catalyst for oxidation, oxidative esterification, hydrodesulfurization and multicomponent (Biginelli) reactions. The PMo_{12} consist of counter proton in secondary structure. This available proton can be exchanged with transition metal to take the advantage of both PMo_{12} and transition metal. A number of articles have been reported on precious transition metals such as Ru [1-6], Pt [1, 3, 4, 6-11], Pd [12-15], Au [16] and Ag [17] exchanged supported phosphomolybdic acid.

Amongst the reported articles, in 2012, Xing group first time reported the preparation of uniform Pd nanoparticles by using phosphomolybdic acid (PMo_{12})-assisted method for synthesis of Pd-PMo_{12}/C catalyst and its catalytic activity was evaluated for electro-catalytic oxidation of formic acid. [12]. In 2013, Dai et al. reported a novel method for synthesis of Pd exchanged phosphomolybdic acid supported on polyaniline (PAN-) functionalized carbon supports (Pd/HPMo-PAN-C) catalyst [13] and its catalytic activity and stability were evaluated for electro-chemical oxygen reduction reaction. Two years later in 2015, Lin group demonstrated green synthesis of PdCu supported on graphene/polyoxometalate LBL films (PdCu@PDDA-GN/PMo_{12}) in two steps [14]. The prepared PdCu@PDDA-GN/PMo_{12} catalyst was utilized for eletrocatalytic activity of formic acid oxidation. After that, in 2016, Yuan et al. reported electro-catalytic oxidation of formic acid by Pd nanoflowers supported phosphomolybdic acid-modified graphene (Pd NF/HPMo-G) catalyst which was prepared by first supporting phosphomloybdic acid on graphene oxide followed by in-situ growth of Pd nanoflowers [15].

Above literature survey shows that only carbon based materials are used as supports but no report is available on metal oxide, for example zirconia, for the same. Therefore, we have synthesized Pd exchanged phosphomolybdic acid supported on zirconia (Pd-PMo_{12}/ZrO_2), characterized and its catalytic activity was evaluated for hydrogenation of styrene, cyclohexene and levulinic acid

under optimized conditions viz., (i) catalyst (5 mg), styrene (10 mmol), EtOH: H_2O (30:20 mL), H_2 pressure (5 bar), time (3 h), temperature (30 °C); (ii) catalyst amount (25 mg), cyclohexene (9.87 mmol), H_2O (50 mL), H_2 pressure (10 bar), time (2 h) and temperature (50 ˚C) and (iii) Catalyst (5 mg), LA (5 mmol), FA (125 mmol), time (6 h), temperature (200 °C) as described in part A (Chapter 1 & 2) and part B (Chapter 1) respectively. The obtained result (99%, 96% and 98% conversation respectively) shows that it is highly active for all three reactions which may be due to the high dispersion of Pd metal, resulting in the formation of Single-atom site catalyst (SASc). SASc is referred as automatically dispersed single metal atoms, isolated metal atoms or ions, molecular complexes, and even clusters located discretely on solid supports in the same way and behave similarly in catalysis[18-21].

Recently, SASc have created tremendous attention in frontier heterogeneous catalysis community because of its promising atom utilization efficiency and unique catalytic activity towards the targeted product selectivity, which play a vital role in industrial chemical synthesis [18-23]. In addition, SASc bridged the gap between homogeneous and heterogeneous catalysis by grasping the inherent dual advantage of both, approximately 100% atomic utilization along with high stability and easy separation from reaction media, recyclability as well as stability respectively [23-25].

However, reducing the size of metal nanoparticles down to single-atomic level has enhanced the surface energy with high mobility [20, 21, 26], which leads to agglomeration by particle coalescence or by Ostwald ripening [27, 28]. Thus, to prevent this, the support or host material must have specific anchoring sites, such as coordinatively unsaturated surface atoms (e.g., O^{2-}, OH^-), surface vacancies, or heteroatom dopants (e.g., N, P, S, and halogens) [29-31], which can stabilize catalytic metal centres as individual atoms via physical or chemical methods [23, 32]. However, to achieve this, physical methods such as mass-selected soft landing [23, 33], defect engineering [34], iced-

photochemistry [35], atomic layer deposition [36], galvanic replacement [37], high temperature migration [38], and high-temperature pyrolysis [39, 40] are not feasible yet because of low yield, and they require highly expensive and complex equipment. On the other hand, wet-chemistry techniques such as impregnation [41], ion-exchange [42], co-precipitation [43] and adsorption methods are more practical to anchor metal atoms on the support via covalent interactions, ionic interactions, or geometric enclosure in small pores [31] and avoid their aggregation during the post-treatment processes. In this direction, till date there are several reports for successful fabrication of SACs on various supports, such as metal hydroxide/oxides [44-47], graphene [48-51], porous nitrogen-doped carbon [52-57], metal-organic frameworks (MOFs) [58-62], and zeolites [63].

From the above viewpoint, metal oxide clusters, particularly Keggin type polyoxometalates (POMs) have attained great attraction in recent years [21, 27, 28, 31]. As discussed in general introduction, PMo_{12} are well-defined anionic inorganic complex comprising highly stable 3D-cage like structure of molecular level molybdenum oxides, which consist of technologically important fascinating physical and chemical properties. Their robust oxoanionic nature, Brønsted acidity, reversible redox behaviour, high stability, reducing and encapsulating ability make them ideal model systems to explore and learn how to stabilize metal oxide anchored SASc.

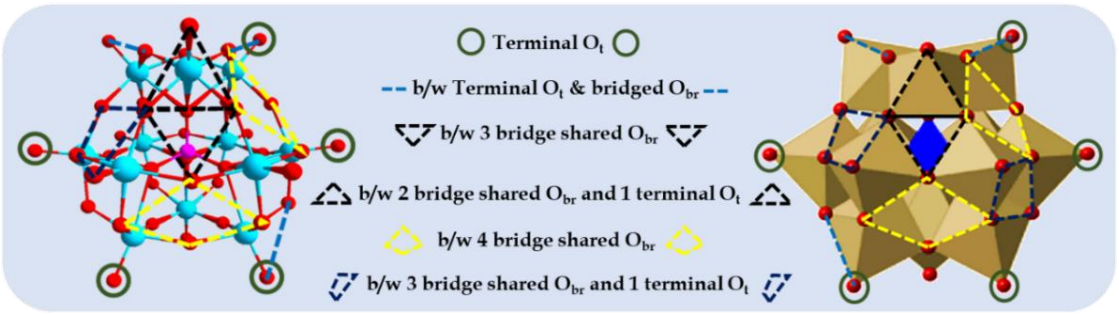

Figure 1. Different types of surface O atoms and possible anchoring sites for Pd atoms on Keggin-structured anion phosphomolybdic acid

Based on structural and chemical diversity, PMo_{12} are mainly divided into two classes for stabilizing SASc [31]. Class I-PMo_{12}-SACs consisting of plenary structure of $[(PMo_{12}O_{40})^{3-}]$ units, which stabilizes single atom outside the shell, geometrically predefined positions for oxo coordination environment and Class II-POM-SACs based on lacunary $[(PM_{12-m}O_{40-m})^{n-}]$ unit, in which single atom is stabilized in lacuna created by removing one or more than one metal-oxo unit from plenary structure. The class I stabilized POM-SACs (Figure 1), contains single corner site (terminal O_t), bridge site (b/w terminal O_t and bridged O_{br}), three-fold hollow sites (i.e., b/w three bridge shared O_{br} and b/w two bridge shared O_{br} and one terminal O_t), and four-fold hollow sites (i.e., b/w four bridge shared O_{br} and b/w two bridge shared O_{br} and two terminal O_t), making POM an ideal stabilizer for SACs [27, 28]. However, most preferable site is expected to be terminal sites as reported by Yan group [27, 28].

In this direction, first time Yan et. al. in 2016, reported phosphomolybdic acid-stabilised $Platinum_1$ single-atom catalyst supported on activated carbon with 0.98 wt% loading of Pt and its catalytic efficiency for hydrogenation of nitrobenzene and cyclohexanone [27]. Based on the DFT calculations, they also confirmed that the four fold coordination site is highly favourable for stabilizing Pt SACs. After three years, in 2019, same group has reported a series of highly dispersed Pt Single atom stabilized by different polyoxometalates (PTA, PMA, STA, SMA) supported on graphene for hydrogenation of propene [28]. By DFT calculations they have found that Pt adsorption energy difference between different POMs was in the order: Pt_1/PTA>Pt_1/PMA>Pt_1/STA>Pt_1/SMA. In 2021, Li et al. reported diboration of phenylacetylene via Pt SASc catalyst stabilised by MOF fabricated phosphomolybdic acid [21]. Thus, literature shows that there is no report available for the synthesis and detailed characterization of phosphomolybdic acid-stabilised Pd single atom site catalyst (SASc).

It is also observed from the literature survey that few reports are available for synthesis of functionalized aminobiphenyl via Tandem Suzuki–Miyaura cross coupling-nitro hydrogenation reaction over Pd based catalysts, such as, $Pd(OAc)_2$ [64], mesoporous silicabis(ethylsulfanyl)propane palladium [65], $[Pd(H_2L)(Cl)_2]$ [66], mannose stabilized Pd [67], PdcNPs/C@Fe_3O_4 [68] and Fe_3O_4@Pd/PDA catalyst [69]. It is worth noting that they have several drawbacks, like use of high amount of catalysts, organic solvents (DMF and IPA), reducing agent ($NaBH_4$ and $N_2H_4.H_2O$), tedious isolation, and deactivation of the catalyst after regeneration.

Looking into the importance of SASc as well as Tandem Suzuki–Miyaura cross coupling-nitro hydrogenation reaction, in this chapter, we reported designing of zirconia supported phosphomolybdic acid stabilised Pd-Single atom site catalyst using simple wet chemistry method (Pd-PMo_{12}/ZrO_2). X-ray photoelectron spectroscopy (XPS) reveal that Pd-PMo_{12}/ZrO_2 contained Pd(0). HRTEM and dark-field scanning transmission electron microscopy (HAADF-STEM) confirmed the presence of automatically dispersed Pd atom. The catalyst efficiency was evaluated for Suzuki–Miyaura cross coupling and Tandem Suzuki–Miyaura cross coupling-nitro hydrogenation reaction, under mild reaction conditions. The influence of various reaction parameters like catalyst amount, reaction time, temperature, pressure and solvent were studied thoroughly. To validate the stability, the catalyst was regenerated and reused up to three cycles. The regenerated catalyst was characterised using EDX, FT-IR, and XPS and plausible reaction mechanism for the reactions were also proposed.

EXPERIMENTAL

Materials

All chemicals used were of A. R. grade. Phosphomolybdic acid, zirconium oxychloride, ammonia, palladium chloride, 1-iodo-2-nitrobenzene,

phenylboronic acid, potassium carbonate and dichloromethane were received from Merck and used as received without further purification.

Catalyst Synthesis

Zirconia supported Phosphomolybdic acid stabilized Pd SASc (Pd-PMo_{12}/ZrO_2) was synthesize in three steps.

Step-1: Synthesis of Zirconia (ZrO_2):

ZrO_2 was synthesized as described in chapter 2 (Part A).

Step-2: Synthesis of phosphomolybdic acid supported on zirconia (PMo_{12}/ZrO_2) by incipient wet impregnation:

PMo_{12}/ZrO_2 was synthesized as described in chapter 2 (Part A).

Step-3: Synthesis of Zirconia supported Phosphomolybdic acid stabilized Pd SASc (Pd-PMo_{12}/ZrO_2) by soaking and post reducing method:

Zirconia supported phosphomolybdic acid stabilized Pd SASc was synthesized by exchanging the available protons of PMo_{12} with Palladium. 1 g PMo_{12}/ZrO_2 was soaked with 25 mL 0.05 M $PdCl_2$ aqueous solution with intermittent stirring for 24 hours. The mixture was filtered, washed with distilled water to remove excess Pd and dried in air at room temperature. The obtained wooden brown colored material was designated as Pd(II)-PMo_{12}/ZrO_2 . Finally, the synthesized material was charged in a Parr reactor for reduction of Pd(II) to Pd(0), under 1 bar H_2 pressure, at 40 °C for 30 min. The obtained grey colored material designated as Pd-PMo_{12}/ZrO_2 (Scheme 1). Similarly using wet-impregnation method other three catalysts, $Pd_{0.2}$-PMo_{12}/ZrO_2, $Pd_{0.45}$-PMo_{12}/ZrO_2 and Pd_1-PMo_{12}/ZrO_2 were synthesized (where 0.2, 0.45 and 1 stands for wt% of Pd).

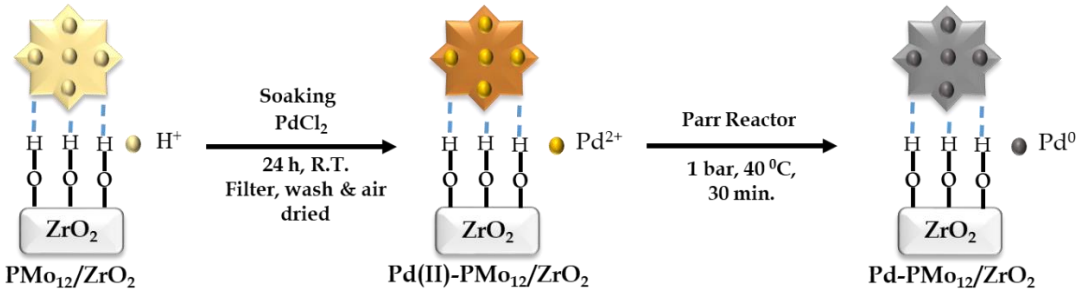

Scheme 1. Synthesis of Pd-PMo_{12}/ZrO_2

Synthesis of $Pd_{(0.2\%/0.45\%/1\%)}$-PMo_{12}/ZrO_2 by incipient wet impregnation method:

A series of catalyst containing of 0.2, 0.45 and 1 Wt% of Pd in zirconia supported phosphomolybdic acid stabilized Pd SASc were synthesized by wet impregnation method. 1 g of PMo_{12}/ZrO_2 was added to aqueous solution of $PdCl_2$ (0.00334/30, 0.00751/30 and 0.0167/30 g mL^{-1} in double distilled water) and dried for 10 hours at 100 °C. The obtained light wooden brown colour material was designated as 0.2%, 0.45% and 1% Pd(II)-PMo_{12}/ZrO_2 respectively. For the reduction of Pd(II) to Pd(0), the resulting material charged in a Parr reactor under 1 bar H_2 pressure, at 40 °C for 30 min. the obtained black colored material designated as $Pd_{0.2}$-PMo_{12}/ZrO_2, $Pd_{0.45}$-PMo_{12}/ZrO_2 and Pd_1-PMo_{12}/ZrO_2 respectively.

Catalytic activity

Suzuki-Miyaura cross-coupling reaction

The Suzuki-Miyaura (SM) cross-coupling reaction was carried out in a 50 mL glass batch reactor on a hot-plate magnetic stirrer as show in scheme 2. The glass batch reactor was filled with aryl halide, phenylboronic acid, K_2CO_3 and EtOH: H_2O as solvent and catalyst. The reaction was carried out at appropriate temperature and time with stirring in oil bathe (Scheme 2). After completion of the reaction, reaction mass was cooled and the organic phase was extracted with dichloromethane. The organic phase was dried with anhydrous magnesium sulfate and analyzed by gas chromatograph (Shimadzu-2014)

using a capillary column (RTX-5). The products were confirmed by comparison with the standard samples.

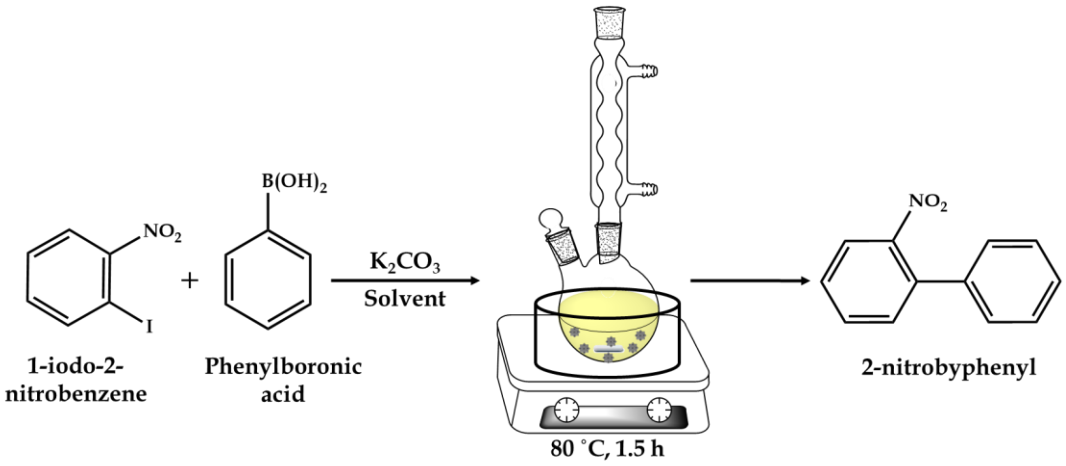

Scheme 2. Schematic presentation of Suzuki-Miyaura cross-coupling reaction

Tandem Suzuki-Miyaura cross-coupling/nitro hydrogenation reaction

The catalytic reaction was performed in the high-pressure autoclave reactor. The reactor vessel was filled with aryl halide, phenylboronic acid, K_2CO_3, EtOH: H_2O as solvent and catalyst for the SM cross-coupling reaction. After completion of SM cross-coupling, for hydrogenation reaction, the presence of air in the reactor vessel's unfilled space is removed by flushing with H_2 gas several times. Finally, appropriate amount of H_2 pressure was applied for the reaction, at SM Cross-coupling reaction temperature with a stirring rate of 500 rpm. The continuous reduction of pressure within the vessel was used to determine the progress of the reaction. After completion, the reaction mixture was cooled to room temperature and then H_2 pressure was released from the vent valve. The schematic representation of catalytic methodology is represented in scheme 3. The organic layer was extracted using dichloromethane, while the catalyst was collected from the liquid phase junction and finally recovered through centrifugation. The organic phase was dried with anhydrous magnesium sulfate and analyzed by gas chromatograph (Shimadzu-2014) using a capillary column (RTX-5). The products were confirmed by comparison with the standard samples.

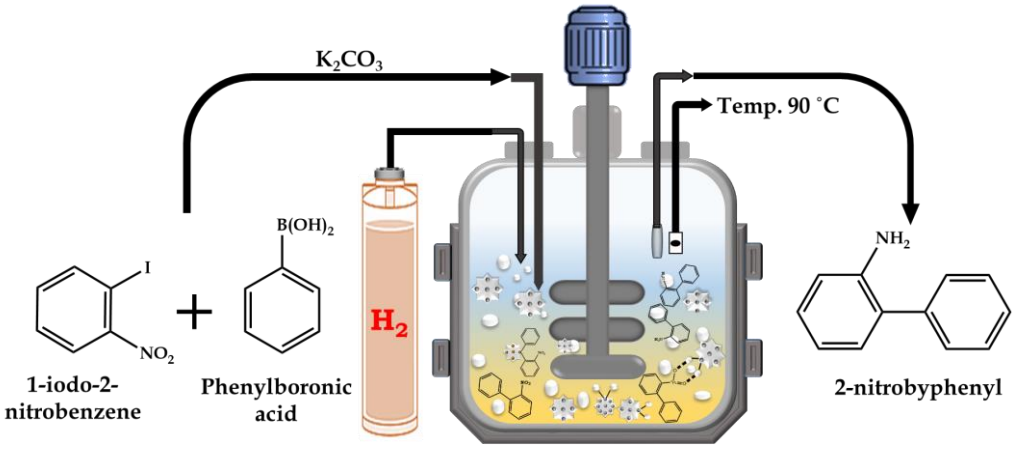

Scheme 3. Schematic representation of Tandem Suzuki-Miyaura cross-coupling/nitro hydrogenation reaction

RESULT AND DISCUSSION

Characterization

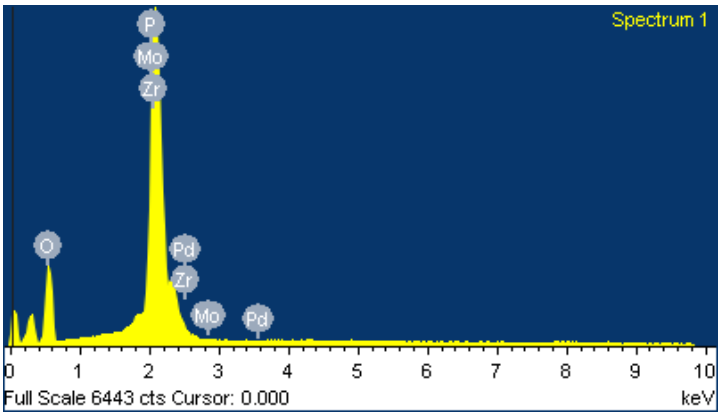

Figure 2. EDX of Pd-PMo_{12}/ZrO_2

In synthesized Pd-PMo_{12}/ZrO_2, the amount of Pd (0.43 wt %) was found by gravimetric analysis of standard solution and filtrate [70-72]. EDX elemental mapping of Pd-PMo_{12}/ZrO_2 (Figure 2) shows presence of all elements i.e., P, Pd, Mo, O, & Zr. The analytical values (Table 1) of Pd and Mo by EDX was found to be 0.45 wt% and 14.01 wt% respectively which is in good agreement with calculated values, Pd (0.43 wt %) and Mo (14.05 wt%). Low % of Pd indicates that only the protons of PMo_{12} were exchanged. Table 1 also shows obtained EDX values of Pd and Mo in $Pd_{0.2}$-PMo_{12}/ZrO_2, $Pd_{0.45}$-PMo_{12}/ZrO_2 and Pd_1-PMo_{12}/ZrO_2 are in good accord with the theoretical calculated values.

It is interesting to note down that all the catalysts consist of <1% Pd, which is the first indication for the presence of Pd Single atom site catalyst [27, 28].

Table 1. EDX analysis

Catalyst	EDX value (wt%)		Theoretical value (wt%)	
	Pd	Mo	Pd	Mo
Pd-PMo_{12}/ZrO_2	0.45	14.01	0.43	14.05
$Pd_{0.2}$- PMo_{12}/ZrO_2	0.19	14.92	0.2	14.9
$Pd_{0.45}$- PMo_{12}/ZrO_2	0.44	13.9	0.45	13.9
Pd_1- PMo_{12}/ZrO_2	0.99	13.49	1	13.5

To support our observation, the SM cross-coupling reaction was carried out using all four synthesized catalysts and obtained results are presented in Table 2. It is observed from Table 2, that for all catalysts (entry 1-4), the % conversion remains same except entry 1. This interesting unique observation made us to keep another set of reactions (Table 2) with exactly same concentration of active Pd (entry 5-7) to achieve maximum % conversion. Above study clearly indicates the presence of Pd as a Single atom site catalyst (SASc). It is also observed that minimum amount of active spices, 0.09 mg is required for maximum conversion. It is interesting to note that the catalyst containing 0.45% Pd is best irrespective of synthesis process (ion exchange by soaking method or impregnation method). However, from the view point of possibility of reusing of $PdCl_2$ solution (filtrate), we have selected the catalyst (Pd-PMo_{12}/ZrO_2) synthesised by ion-exchange method for further detailed characterization as well as catalytic study. ICP analysis of Pd-PMo_{12}/ZrO_2 was carried out and obtained values (0.46 wt% and 14.15 wt% for Pd and Mo respectively), are in good agreement with the values obtained from theoretically and EDX analysis.

Table 2. Effect of Pd amount

Entry	Catalyst	Catalyst amount (mg)	Active amount of Pd mg (mmol)	% Conversion
1	$Pd_{0.2}$-PMo_{12}/ZrO_2	20	0.04 (0.37* 10^{-3})	73
2	Pd-PMo_{12}/ZrO_2	20	0.09 (0.84* 10^{-3})	>99
3	$Pd_{0.45}$-PMo_{12}/ZrO_2	20	0.10 (0.94* 10^{-3})	>99
4	Pd_1-PMo_{12}/ZrO_2	20	0.20 (1.87* 10^{-3})	>99
5	*$Pd_{0.2}$-PMo_{12}/ZrO_2	40	0.08 (0.37* 10^{-3})	99
6	**$Pd_{0.2}$-PMo_{12}/ZrO_2	45	0.08 (0.37* 10^{-3})	>99
7	***Pd_1-PMo_{12}/ZrO_2	9	0.09 (0.84* 10^{-3})	>99

Reaction conditions: Catalyst (20 mg, *40 mg, **45 mg and ***9mg), 1-iodo-2-nitrobenzene (1.96 mmol), phenylboronic acid (2.94 mmol), K_2CO_3 (3.92 mmol), EtOH: H_2O (5:5 mL), time (2 h), temperature (90 °C).

The thermal stability of PMo_{12}/ZrO_2 and Pd-PMo_{12}/ZrO_2 was determined using TGA (Figure 3). TGA curve of PMo_{12}/ZrO_2 shows (Figure 3) 5.3% weight loss up to 100 ˚C, which is attributed to the loss of adsorbed water. Further, it shows 6.4% weight loss up to 300 ˚C corresponds to the loss of crystalline water molecules present in PMo_{12}. After that, no further weight loss up to 500 ˚C indicates the stability of PMo_{12}/ZrO_2. The TGA of Pd-PMo_{12}/ZrO_2 show 9.3% weight loss up to 200 ˚C which should be attributed to the loss of adsorbed crystalline water molecule. Besides this no significant weight loss was observed up to 500 ˚C indicating the high thermal stability of the catalyst.

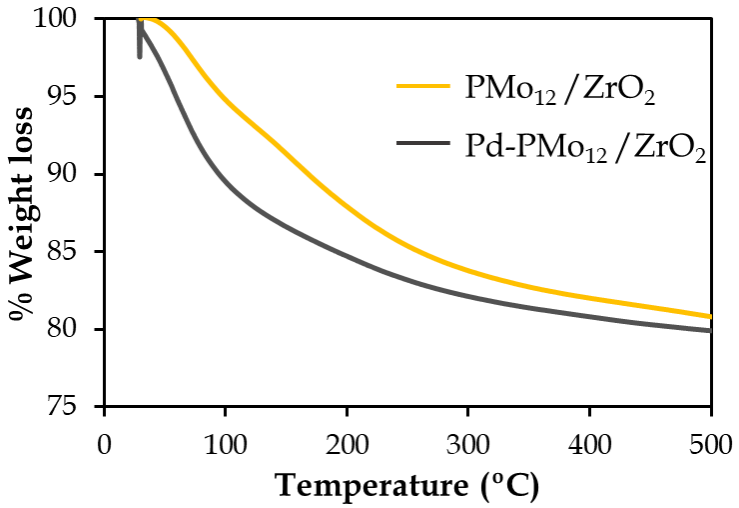

Figure 3.TGA curve of PMo_{12}/ZrO_2 and Pd-PMo_{12}/ZrO_2

The FT-IR spectra of ZrO_2, PMo_{12}, PMo_{12}/ZrO_2, and Pd-PMo_{12}/ZrO_2 are displayed in figure 4. As shown in figure 4a, ZrO_2 show bands in the region of 1600 and 1370 cm^{-1} corresponding to H–O–H and O–H–O bending and a broad band at 600 cm^{-1} corresponding to Zr–O-H bending [70, 71]. PMo_{12} show (Figure 4b) four characteristic bands of Keggin unit at 1060, 965, 870 and 790 cm^{-1} corresponding to the central P-O, terminal Mo=O, and corner shared and edge shared Mo-O-Mo stretching, respectively [73]. FT-IR spectra of PMo_{12}/ZrO_2 (Figure 4c) shows all the characteristic band of PMo_{12} at 1063, 965, 870 and 790 cm^{-1} as well as ZrO_2 at 1605, 1381 and 600 cm^{-1}, without significant change, which indicates the retention of Keggin unit in the synthesized material. The FT-IR spectrum of Pd-PMo_{12}/ZrO_2 (Figure 4d) show all bands corresponding to PMo_{12}/ZrO_2 (1078, 956, 878, 1605, 1381 and 600 cm^{-1}) with slight shifting, which is attributed to the replacement of counter cation protons of PMo_{12} by Pd. Here, band corresponding to Pd–O band (654 cm^{-1}) is not observed, may be due to superimposition with that of broad band corresponding to Zr-O-H. The obtained spectra confirm the Pd only gets exchanged with the proton of PMo_{12}. If Pd would have been into the lacuna, it would have shown splitting in P-O band. However, since no splitting was observed which indicates that Pd does not get into lacuna.

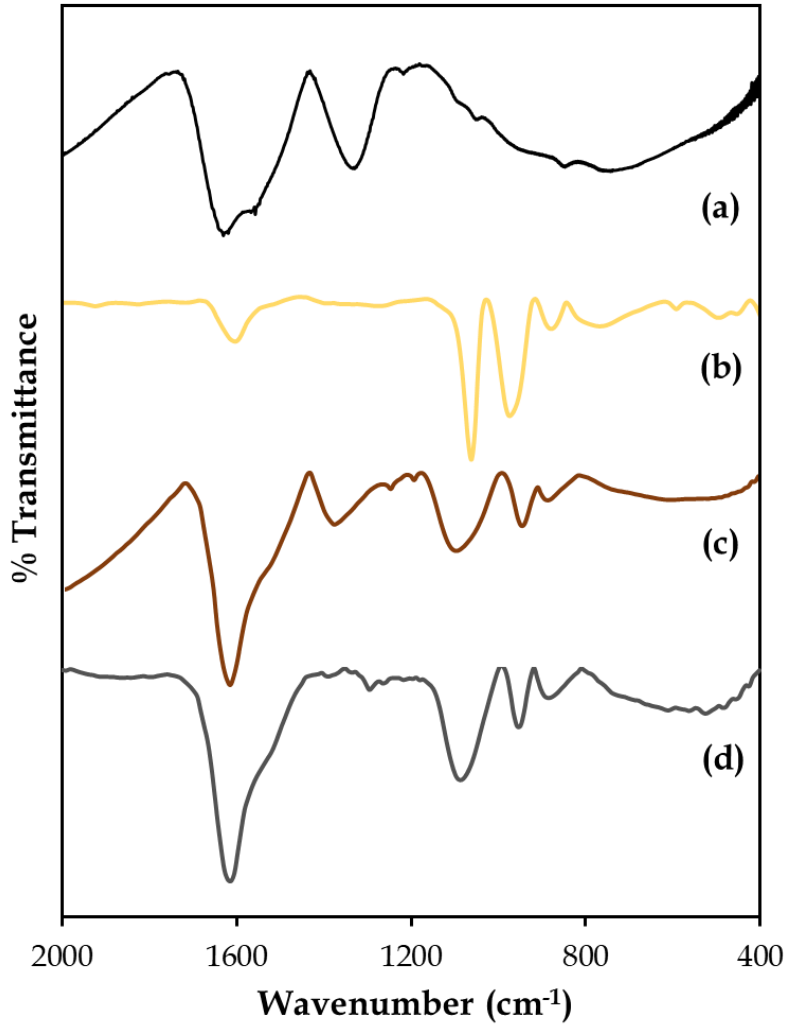

Figure 4. FT-IR spectra of (a) ZrO_2, (b) PMo_{12}, (c) PMo_{12}/ZrO_2 and (d) Pd-PMo_{12}/ZrO_2

^{31}P MAS NMR of PMo_{12}, PMo_{12}/ZrO_2 and Pd-PMo_{12}/ZrO_2 was carried out to understand the chemical environment around central phosphorus atom in PMo_{12} as well as the interaction of the anion with support. ^{31}P NMR of pure PMo_{12} show (Figure 5a) a single intense peak at -3.8 ppm and is in good agreement with the reported ones [73, 74]. Moreover PMo_{12}/ZrO_2 showed (Figure 5b) a slight up filed shifting in peak from -3.8 to -4.1 ppm which may be due to the strong chemical interaction between terminal oxygen (O_t) of PMo_{12} and surface of ZrO_2 . Furthermore, Pd-PMo_{12}/ZrO_2 also show (Figure 3c) significant up filed shifting in peak from -4.1 to -5.61 ppm. This is due to change in electronic environment of PMo_{12} as Pd gets exchanged with counter proton of PMo_{12}/ZrO_2 which is good agreement with reported one [27, 28].

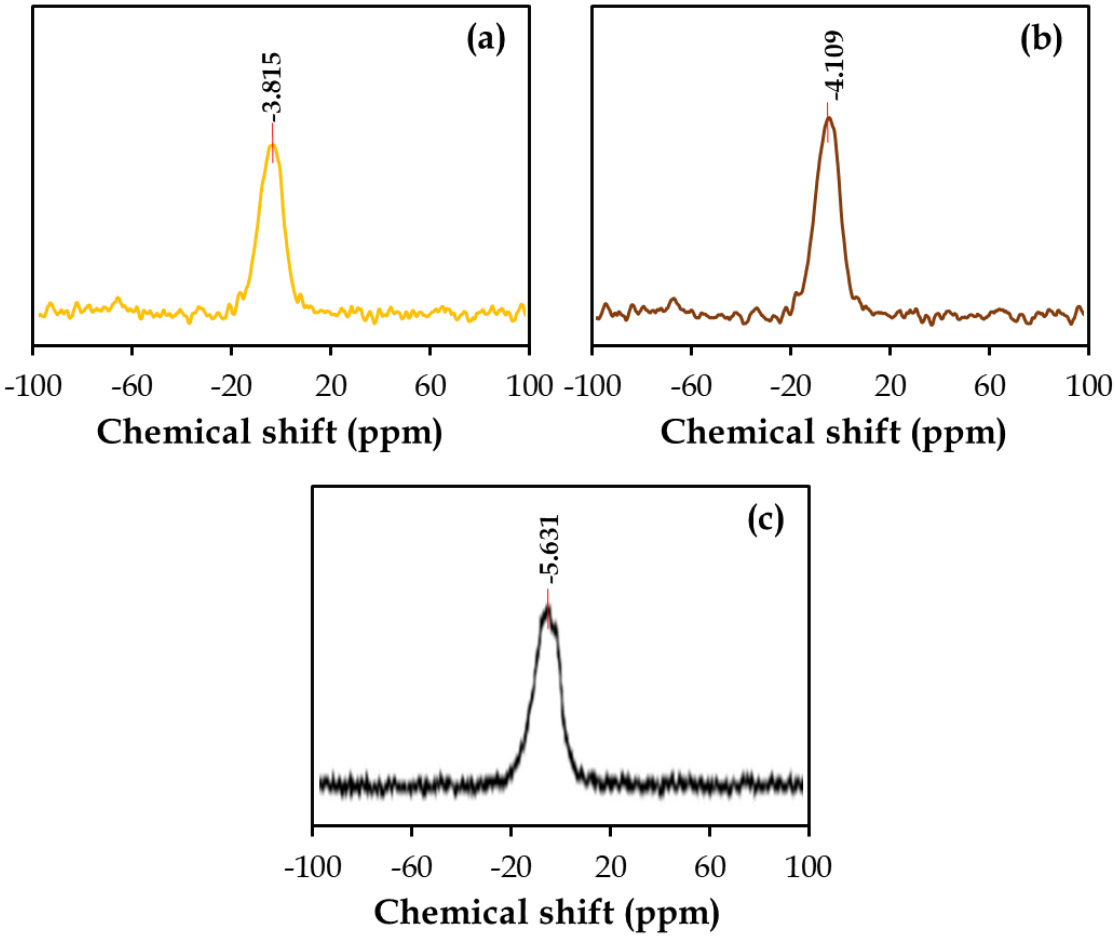

Figure 5. ^{31}P MAS NMR of (a) PMo_{12}, (b) PMo_{12}/ZrO_2 and (c) $Pd\text{-}PMo_{12}/ZrO_2$

XPS spectra of $Pd\text{-}PMo_{12}/ZrO_2$ was carried out to elucidate the oxidation states of Zr, Pd, O and Mo. In figure 6a and b, two higher binding energy peaks at 331 and 345 eV attributes to $Zr3p_{3/2}$ and $Zr3p_{1/2}$ respectively which confirms that Zr is present in +4 oxidation state [70-72, 75]. It also shows (Figure 6a) a highly intense peak at 532 eV corresponding to spin orbit O1s for oxygen present in PMo_{12} as well as in ZrO_2. Figure 6b displays two peaks at 334.78 and 340.16 eV corresponding to two distinct spin-orbits $3d_{5/2}$ and $3d_{3/2}$ attributed to metallic palladium (Pd^0) [25, 70-72, 76] confirming the presence of the same in the synthesized catalyst. Figure 6c shows the two intense peaks at 233 and 235 eV corresponding to spin-orbits $3d_5/2$ and $3d_{3/2}$, of Mo respectively and confirms that Mo(VI) has not reduced during reduction of Pd(II) to Pd(0).

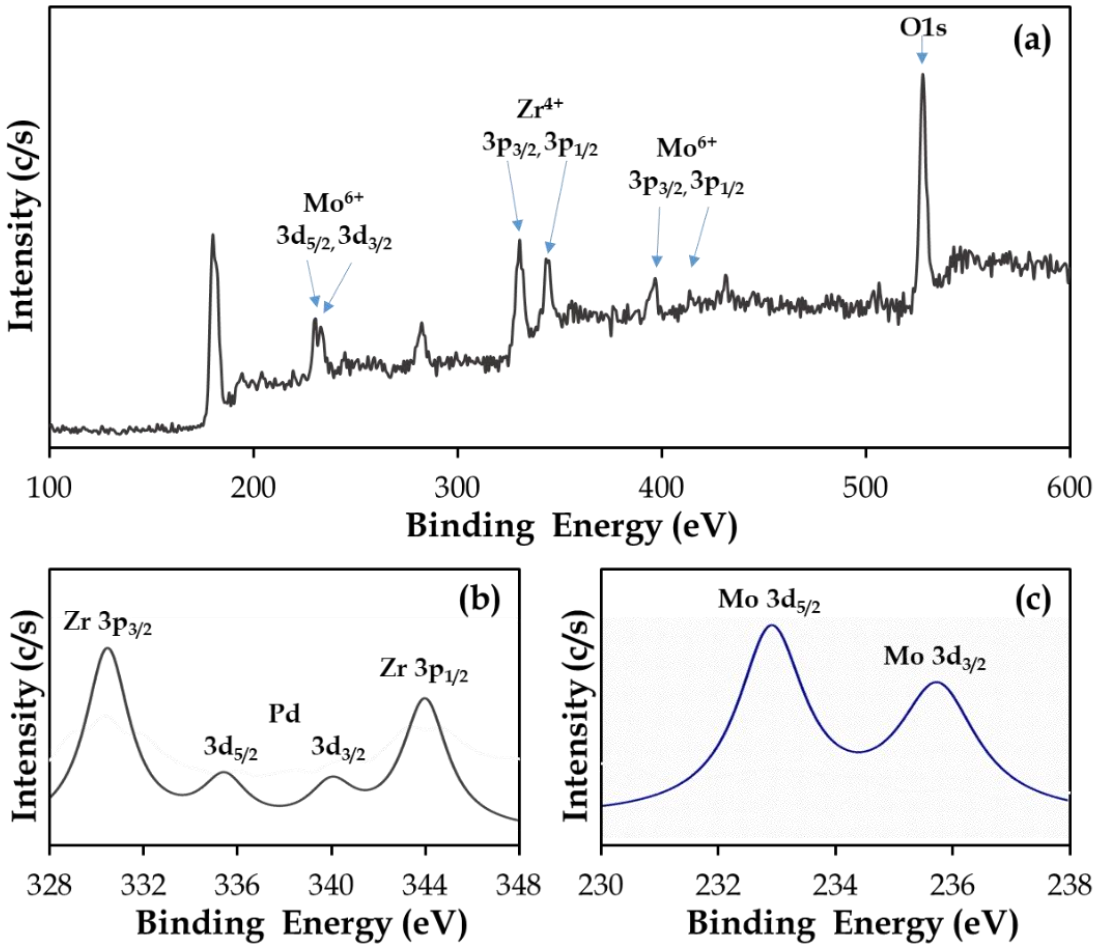

Figure 6. XPS of Pd-PMo_{12}/ZrO_2

The N_2 sorption isotherms of ZrO_2, PMo_{12}/ZrO_2, Pd(II)-PMo_{12}/ZrO_2, and Pd-PMo_{12}/ZrO_2 are shown in figure 7. The obtained unaltered nature of N_2 adsorption desorption isotherms for ZrO_2 and synthesized catalyst confirms that even after supporting PMO_{12} and reduction of Pd on the surface of ZrO_2, the basic structure is retained. The BET surface area of ZrO_2 was found to be 170 m^2g^{-1} [70-72]. As expected, the significant higher surface area was obtained in case of PMo_{12}/ZrO_2 (204 m^2 g^{-1}) is due to strong interaction between PMo_{12} and ZrO_2. However, a slight increase in surface area from 204 to 208 m^2g^{-1} in case of Pd(II)-PMo_{12}/ZrO_2 was due to exchange of Pd with available protons of PMo_{12} over PMo_{12}/ZrO_2. Further, drastic increase in the surface area of Pd(0)-PMo_{12}/ZrO_2 (from 208 to 228 m^2g^{-1}) [70-72] is because of formation of the palladium SASc.

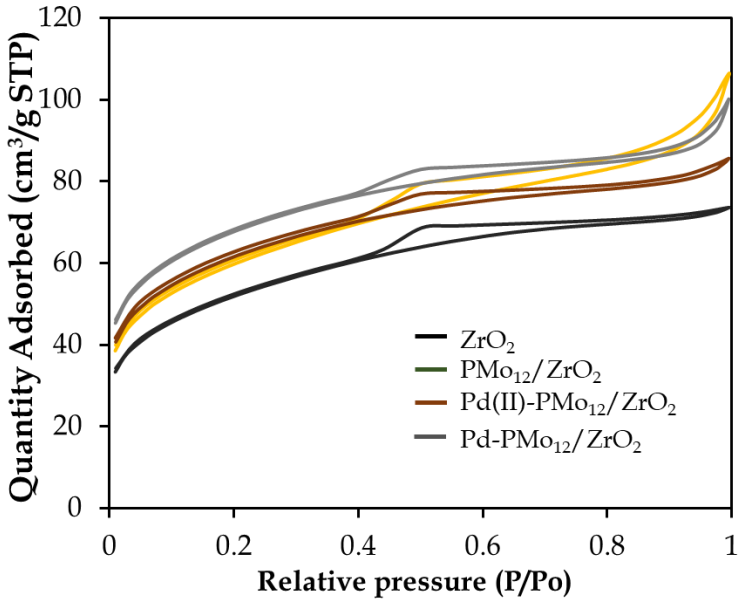

Figure 7. N_2 sorption isotherms ZrO_2, PMo_{12}/ZrO_2, Pd(II)-PMo_{12}/ZrO_2 and Pd-PMo_{12}/ZrO_2

To study the surface morphology, powder XRD pattern of ZrO_2 support, PMo_{12}, PMo_{12}/ZrO_2 and the synthesised Pd-PMo_{12}/ZrO_2 catalyst are shown in figure 8. The figure 8a show characteristic broad peaks between 25°- 35° indicating the amorphous nature of the ZrO_2 support [70-72]. Whereas, PMo_{12} show (Figure 8b) characteristic peaks between 2θ range of 20° to 35° [73]. The powder XRD pattern of PMo_{12}/ZrO_2 does not show (Figure 8c) any characteristics diffraction peaks of PMo_{12}, which indicates that PMo_{12} is highly dispersed as non-crystalline form on ZrO_2. The XRD pattern of Pd-PMo_{12}/ZrO_2 (Figure 8d) does not show any corresponding characteristic planes of Pd and it is similar to PMo_{12}/ZrO_2. The obtained results suggest that the amount of Pd (0.45 %wt) is beyond detection limit of powder XRD due to its high degree of dispersion [27, 28], which is further confirmed by HRTEM and HAADF-STEM image.

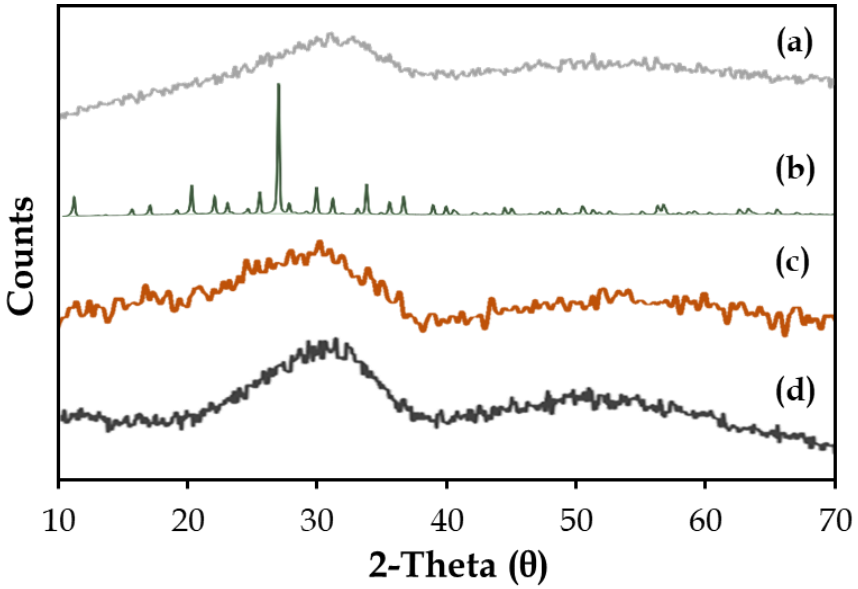

Figure 8. Powder XRD of (a) ZrO_2, (b)PMo_{12} and (c) Pd-PMo_{12}/ZrO_2

The transmission electron microscope (TEM) images of PMo_{12}/ZrO_2, Pd/ZrO_2 and Pd-PMo_{12}/Zro_2 with different magnification are shown in figure 9. As expected PMo_{12}/ZrO_2 show (Figure 9a-c) high dispersion of PMo_{12} on ZrO_2 without agglomeration. Whereas, the TEM images of Pd/ZrO_2 show (Figure 9d-f) metallic Pd(0) nanoparticles with agglomeration. For Pd-PMo_{12}/ZrO_2, neither Pd nanoparticle nor nano cluster could be seen in TEM images (Figure 9g-i), since from EDX and ICP it is shown that 0.45 wt% of Pd is loaded in synthesized catalyst which suggest that the size of Pd particles is beyond the detection limit of TEM [27, 28]. The high-resolution transmission electron microscopy (HR-TEM) images of Pd in Pd-PMo_{12}/ZrO_2 (Figure 9j-l) show a distinct fringe spacing of 0.226 nm which matches with the inter planner spacing (crystallographic plane) (111) generated from the fast Fourier transform pattern of the crystal lattices produced at the diffraction spots in the horizontal direction to the alignment of fringes [76, 77].

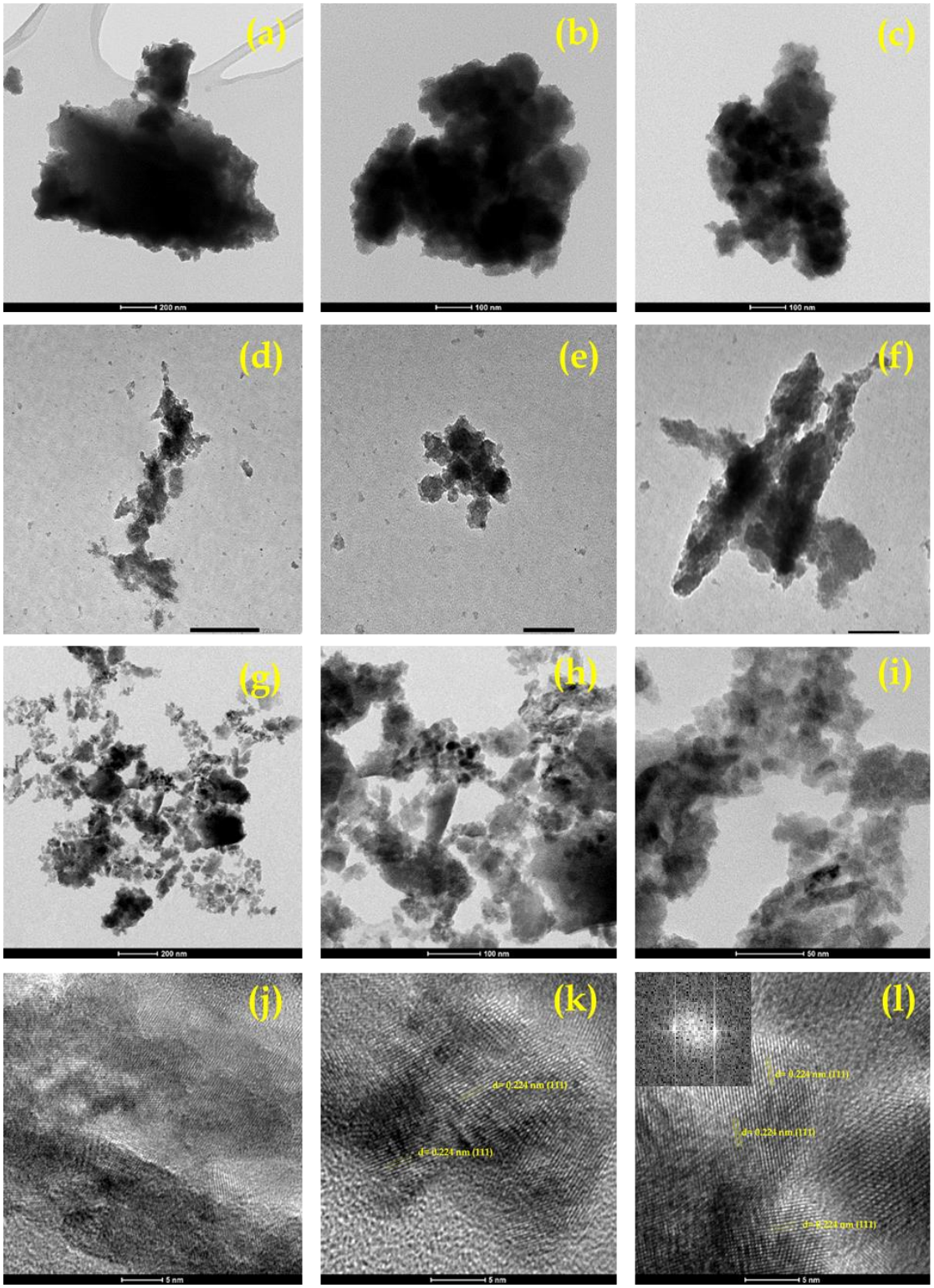

Figure 9. TEM images of (a-c) PMo_{12}/ZrO_2, (d-f) Pd/ZrO_2, (g-i) $Pd\text{-}PMo_{12}$ and (j-l) HRTEM of $Pd\text{-}PMo_{12}/ZrO_2$

To verify the presence of atomically dispersed palladium single atoms, aberration corrected high-angle annular dark-field scanning transmission

electron microscope (AC HAADF-STEM) with coupled EDX analysis measurements were performed (Figure 10). HAADF- STEM images (Figure 10a) show homogeneous dispersion of Pd SACs on the PMo_{12}/ZrO_2 surface. Similarly, EDX elemental mapping of Pd (Figure 10b-f) clearly shows the presence of highly dispersed isolated Pd SACs without any aggregation to form nanoparticle or nano-cluster. Whereas, elemental overlapping images (Figure 10g) indicate that agglomeration of high surface free energy of Pd SACs was efficiently prevented by the electrostatic repulsive interactions derived from PMo_{12} anions as well as high surface area.

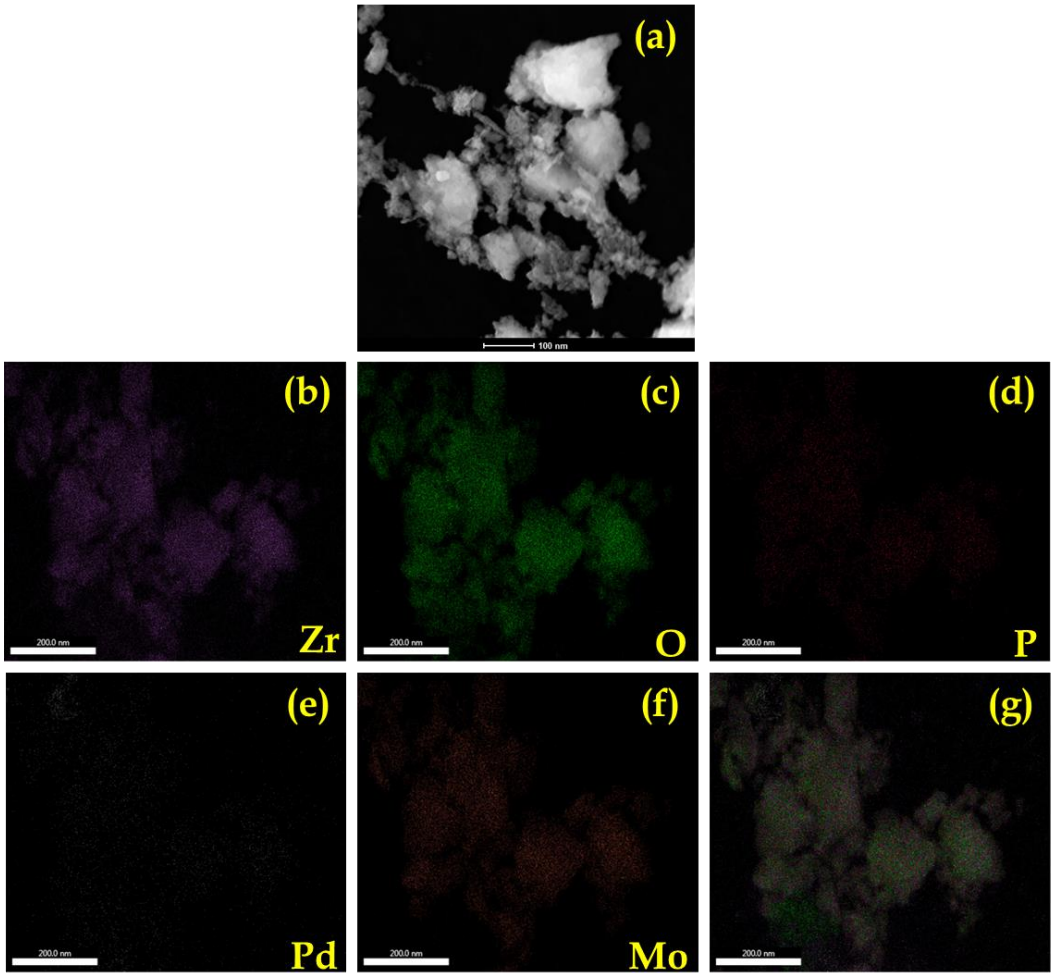

Figure 10. (a) HAADF–STEM and (b-g) EDX of Pd-PMo_{12}/ZrO_2

In summary, FT-IR and ^{31}P MAS NMR showed the retention of Keggin unit after reduction of Pd(II) to Pd(0) in the catalyst. XPS confirm the presence of

Pd(0) and Mo(VI). TEM, HRTEM and STEM indicated the presence of highly dispersed isolated single Pd atoms site (0.226 nm) over the surface of the PMo_{12}/ZrO_2.

Catalytic activity

Suzuki-Miyaura cross-coupling

The catalyst, Pd-PMo_{12}/ZrO_2 was evaluated for SM cross-coupling reaction by varying different reaction parameters such as amount of catalyst, effect of solvent, effect of base concentration, time and temperature to optimize for maximum conversion of 2-nitrobiphenyl.

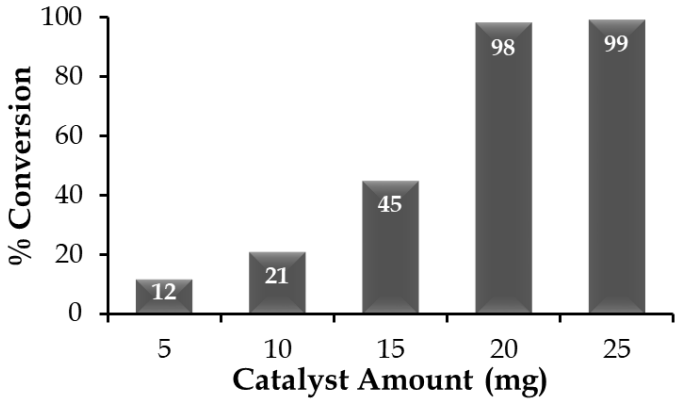

Figure 11. Reaction conditions: 1-iodo-2-nitrobenzene (1.96 mmol), phenylboronic acid (2.94 mmol), K_2CO_3 (3.92 mmol), EtOH: H_2O (5:5 mL), time (2 h), temperature (90 °C).

The catalyst amount was varied from 5 mg to 25 mg and obtained results (Figure 11) indicate that %conversion increases with increasing catalyst amount up to 20 mg because the number of Pd active site increases with respect to substrate concentration. On further increasing catalyst amount up to 25mg, %conversion remains unaltered. As we assume that the synthesized catalyst is Single atom site, to confirm this we have performed experiment to achieve maximum conversion by keeping the amount of catalyst same (5, 10 and 15 mg) and varying the reaction time. The obtained results are shown in Table 3. It is seen that, 99% conversion was achieved on increasing time up to 5, 4, and 3h against each catalyst amounts (5, 10 and 15 mg), which previously gave 15, 21

and 45% conversion respectively. Based on the obtained results, 20 mg of catalyst was optimized for further optimization studies.

Table 3. Effect of time on % conversion

Catalyst	Catalyst amount	Time	% Conversion
Pd-PMo_{12}/ZrO_2	5	5	>99
	10	4	>99
	15	3	>99

Reaction conditions: 1-iodo-2-nitrobenzene (1.96 mmol), phenylboronic acid (2.94 mmol), K_2CO_3 (3.92 mmol), EtOH: H_2O (5:5 mL), temperature (90 ˚C).

It is well known that, the solubility of reactant plays a crucial role on reaction progression and hence different solvents were explored with keeping other parameters constant. From the table 4, it is observed that neat organic solvents like acetonitrile, toluene, DMF and H_2O shows negligible conversion (15%, 6%, 1% and 15% respectively) compared to EtOH (52%). Further, to find the on-water effect [78] on %conversion, reaction was carried out in biphasic solvent system due to its advantages such as i) aqueous water basic phase consisting ionized phenyl boronic acid and ii) aqueous-organic phase with lower pH containing organic component (1-iodo-2-nitrobenzene). The SM cross-coupling reaction occurs at water-organic interphase, neither in water nor in organic phase. It is observed from the table that the reactions carried out with toluene: H_2O and DMF: H_2O solvent system gives negligible increase in the % conversion (24% and 5% respectively). However, when the reaction was carried out with acetonitrile: H_2O and EtOH: H_2O solvent systems, it gives 98% and 99% conversion respectively. Based on the obtained results, environmentally more green solvent system (EtOH: H_2O) was selected for further study.

Table 4. Effect of solvent

Solvent name	Solvent amount (mL)	% Conversion
Acetonitrile	10	15
Toluene	10	6
DMF	10	1
Ethanol	10	58
H_2O	10	15
Acetonitrile: H_2O	5: 5	94
Toluene: H_2O	5: 5	24
DMF: H_2O	5: 5	5
EtOH: H_2O	5: 5	>99

Reaction conditions: catalyst (20 mg), 1-iodo-2-nitrobenzene (1.96 mmol), phenylboronic acid (2.94 mmol), K_2CO_3 (3.92 mmol), time (2 h) and temperature (90 °C).

The effect of EtOH: H_2O ratio was also studied and obtained results are presented in figure 12a. From the results, it can be seen that on changing the solvent system from neat ethanol to EtOH: H_2O ratios (7:3 mL and 5:5 mL), there was increase in %conversion. This trend was observed because of increased solubility of the base in water. However, on further changing the EtOH: H_2O ratio (3:7 mL), the %conversion decreased and very low conversion was observed in neat H_2O because of the poor solubility of organic substrates.

The effect of various organic-inorganic bases on the reaction rate were also studied and the obtained results are shown in figure 12b. The study indicates that the organic base triethyl amine (Et_3N) gave negligible conversion (5%) as compared to the inorganic bases. After use of different inorganic bases, the trend in %conversion was found to be: K_3PO_4 (69%) < NaOH (76%) < Na_2CO_3 (85%) < K_2CO_3 ≈ Cs_2CO_3 (99%). The highest conversion (99%) was obtained with K_2CO_3 and Cs_2CO_3, but for further studies we have selected K_2CO_3 because it is environmentally benign compared to Cs_2CO_3.

To achieve highest conversion, influence of the reaction time was also monitored and obtained results are displayed in figure 12c. From the figure, it

is seen that with increase in time from 0.5 h to 1.5 h, within an interval of 30 min, % conversion increases gradually, which is in good agreement with the well-known fact that with increase in time, there is increase in formation of reactive intermediates from reactants which results into product. Further on prolonging the time up to 2 h, no significant change was observed in the % conversion. Therefore, 1.5 h was optimized with 98% conversion for further optimization of temperature.

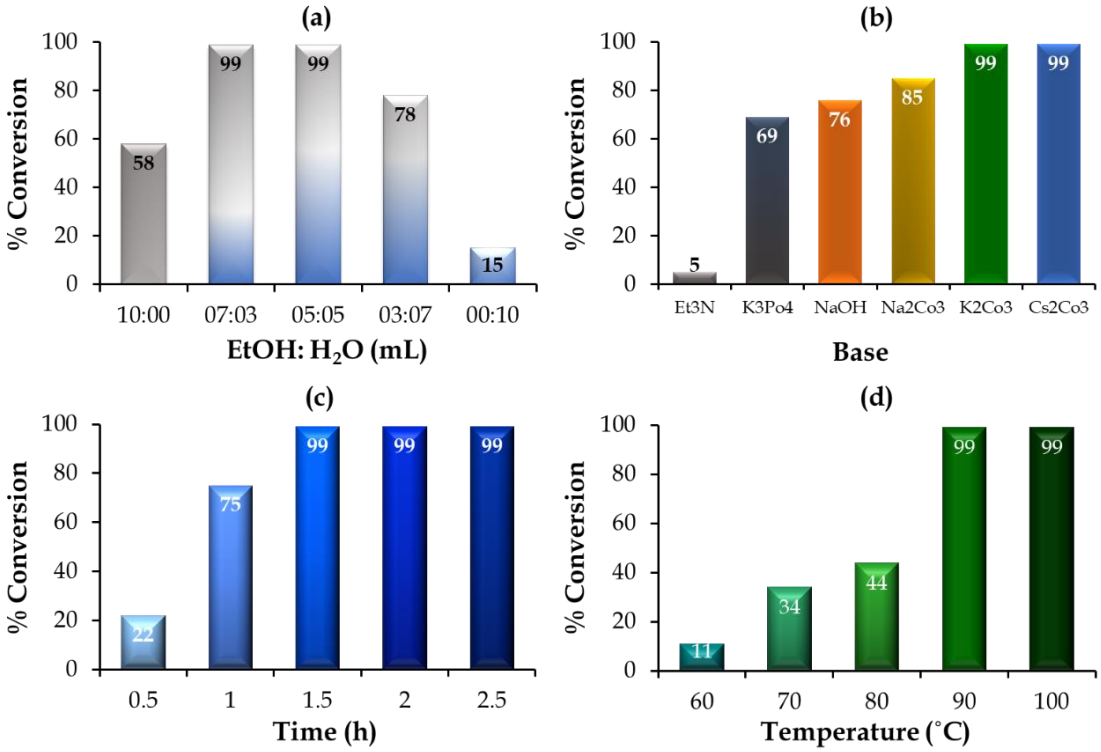

Figure 12. Optimization of reaction parameters for SM cross-coupling. Reaction conditions: (a) Effect of EtOH: H_2O- Catalyst (20 mg), 1-iodo-2-nitrobenzene (1.96 mmol), phenylboronic acid (2.94 mmol), K_2CO_3 (3.92 mmol), time (2 h) and temperature (90 °C); (b) Effect of base- Catalyst (20 mg), 1-iodo-2-nitrobenzene (1.96 mmol), phenylboronic acid (2.94 mmol), EtOH: H_2O (5:5 mL), time (2 h), temperature (90 °C); (c) Effect of Time- Catalyst (20 mg), 1-iodo-2-nitrobenzene (1.96 mmol), phenylboronic acid (2.94 mmol), EtOH: H_2O (5:5 mL), K_2CO_3 (3.92 mmol), temperature (90 °C); (d) Effect of temperature. Catalyst (20 mg), 1-iodo-2-nitrobenzene (1.96 mmol), phenylboronic acid (2.94 mmol), EtOH: H_2O (5:5 mL), K_2CO_3 (3.92 mmol), time (1.5 h).

The effect of temperature on the formation of C-C bond between 1-iodo-2-nitrobenzene, and phenylboronic acid was also investigated for best catalytic

performance with an interval of 10 °C in the range of 90–60 °C. From the figure 12d, it can be seen that on increasing temperature, % conversion increases gradually up to 90 °C. Based on this, 90 °C temperature was optimized to achieve 99% conversion.

Based on this study, the optimized conditions for 99% conversion with TON (2294) and TOF (1529) are: catalyst (20mg), active amount of Pd (0.09mg), 1-iodo-2-nitrobenzene (1.96 mmol), phenylboronic acid (2.94 mmol), EtOH: H_2O (5:5 mL), K_2CO_3 (3.92 mmol), 1.5 h, 90 °C with substrate ratio/ catalyst (2317/1).

The gas chromatographs of starting material and after Suzuki-Miyaura cross-coupling reaction in their respective optimized conditions are shown below in figure 13 and figure 14.

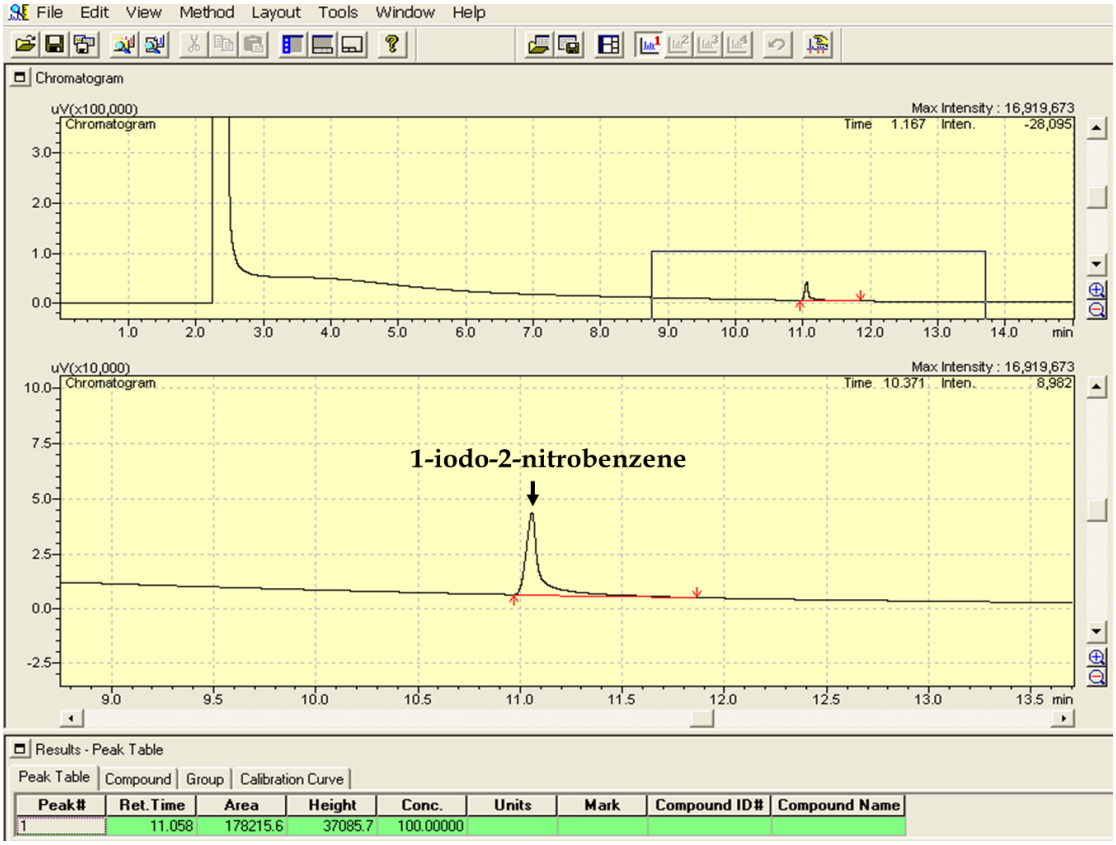

Figure 13. Gas chromatograph of 1-iodo-2-nitrobenzene

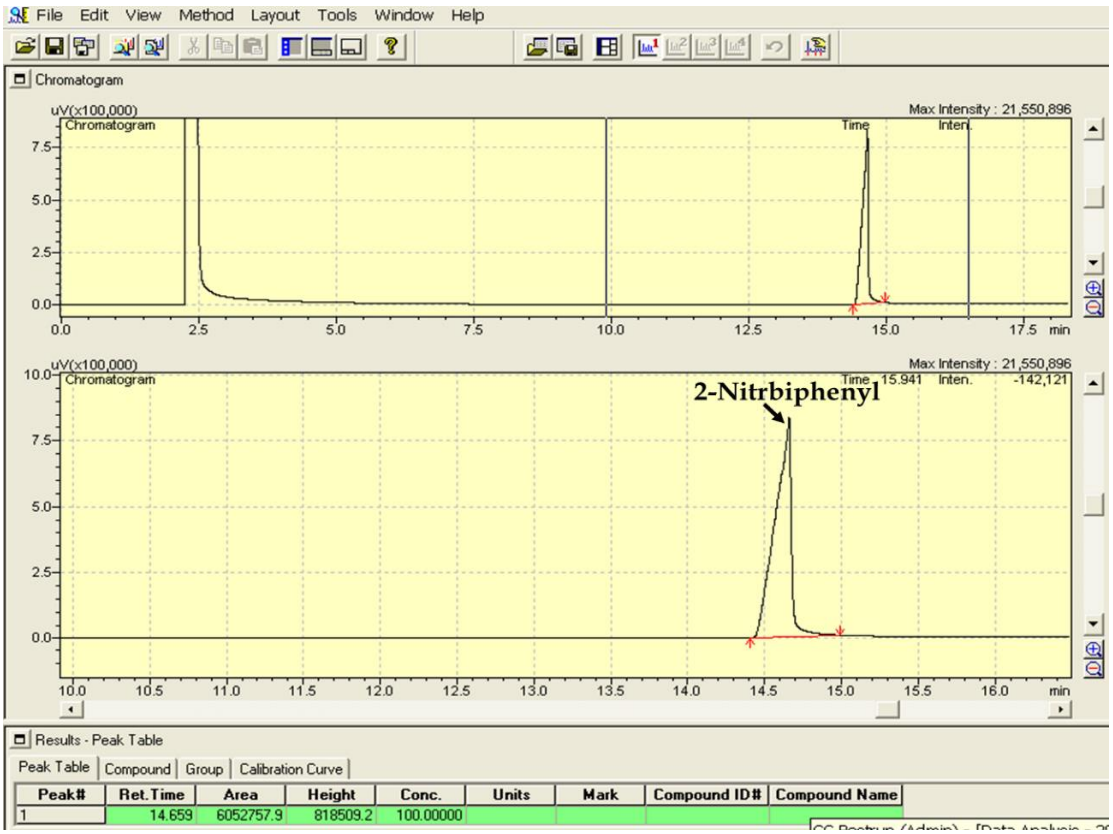

Figure 14. Gas chromatograph of Suzuki-Miyaura cross-coupling

Tandem Suzuki-Miyaura cross-coupling/ nitro hydrogenation reaction

Based on excellent activity of Pd-PMo_{12}/ZrO_2 for SM cross-coupling of 1-iodo-2-nitrobenzene to 2-nitrobiphenyl as well as looking into the importance of nitro hydrogenation reaction, it was thought to merge mechanistically two different catalytic transformations into a single tandem process. We have first applied SM cross-coupling for 1.5 h in high-pressure autoclave at 90 °C, after that H_2 pressure was applied and reaction was continued for 24h (Scheme 5).

The catalyst amount was screened from 20 to 50 mg to achieve maximum conversion and selectivity for hydrogenated product, 2-aminobiphenyl, as shown in figure 15a. Obtained results show that 100% conversion was achieved with 20 mg but the selectivity of 2-aminobiphenyl was only 58%. The lower selectivity of 2-aminobiphenyl obtained might be due to difficulty in approaching NO_2 group of 2-nitrobiphenyl by Pd or due to the conformation of two phenyl rings. Further on increasing the amount of catalyst up to 50 mg,

100% conversion was obtained as well as the selectivity of 2-aminobiphenyl gradually increased because higher amount of Pd was available to react with the reactant species at one time. Therefore, 50 mg of catalyst was optimized for further studies.

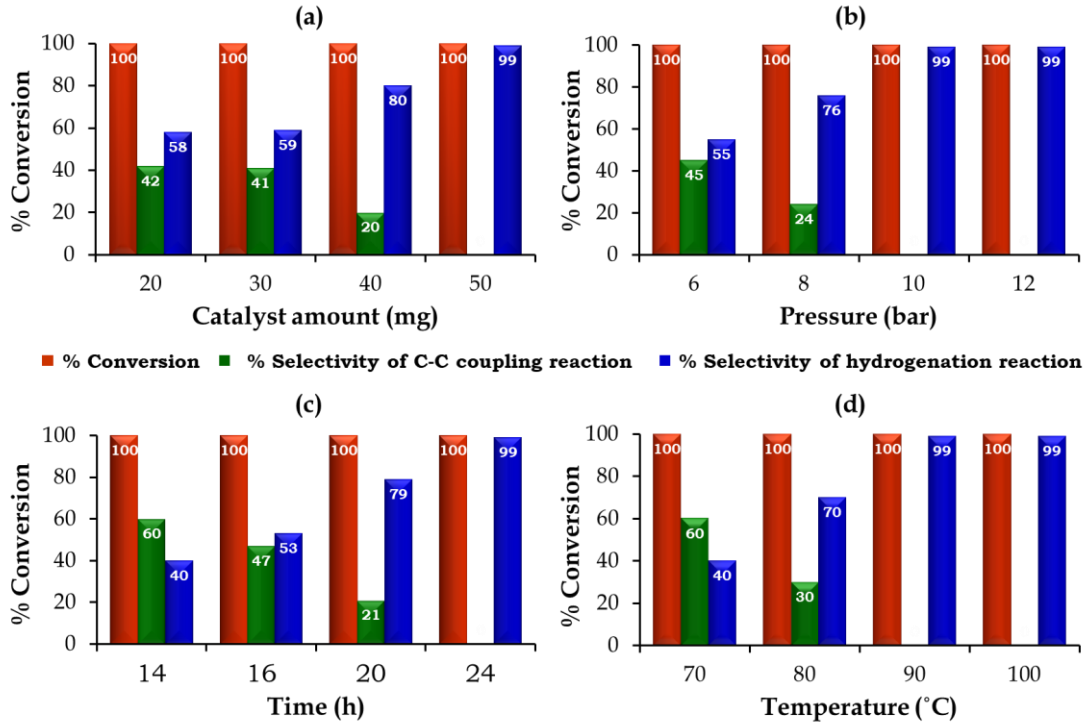

Figure 15. Optimization of reaction parameters for Tandem SM cross-coupling/ nitro hydrogenation reaction. Reaction conditions: (a) Effect of catalyst amount- 1-iodo-2-nitrobenzene (1.96 mmol), phenylboronic acid (2.94 mmol), K_2CO_3 (3.92 mmol), EtOH: H_2O (5:5 mL), pressure (10 bar), time (24 h) and temperature (90 °C); (b) Effect of pressure- Catalyst (50 mg), 1-iodo-2-nitrobenzene (1.96 mmol), phenylboronic acid (2.94 mmol), K_2CO_3 (3.92 mmol), EtOH: H_2O (5:5 mL), time (24 h) and temperature (90 °C); (c) Effect of time- Catalyst (50 mg), 1-iodo-2-nitrobenzene (1.96 mmol), phenylboronic acid (2.94 mmol), K_2CO_3 (3.92 mmol), EtOH: H_2O (5:5 mL), pressure (10 bar) and temperature (90 °C); (d) effect of temperature. Catalyst (50 mg), 1-iodo-2-nitrobenzene (1.96 mmol), phenylboronic acid (2.94 mmol), K_2CO_3 (3.92 mmol), EtOH: H_2O (5:5 mL), pressure (10 bar) and time (24 h).

The influence of H_2 pressure plays an important role for the catalytic transfer hydrogenation reaction. Therefore, the effect of H_2 pressure was also studied and the obtained results are shown in figure 15b. From the Figure, it can be seen that selectivity of hydrogenated product increases gradually on increasing

pressure from 6 to 10 bar. Based on the results, 10 bar pressure was optimized to achieve 100% conversion with 99% selectivity of 2-aminobiphenyl.

Similarly, effect of time and temperature on reaction rate were also investigated to achieve maximum conversion with selectivity of 2-aminobiphenyl and obtained data is shown in Figure 15c & d.

Based on above study, the optimized conditions for 100% conversion with 99% selectivity of 2-aminobiphenyl are: catalyst (50mg), active amount of Pd (0.225 mg), 1-iodo-2-nitrobenzene (1.96 mmol), phenylboronic acid (2.94 mmol), K_2CO_3 (2.96 mmol), EtOH: H_2O (5:5 mL), pressure (10 bar), time (24 h) and temperature (90 °C) with, TON (918), TOF (38) and substrate ratio/ catalyst (927).

The gas chromatographs of optimized reaction condition for Tandem SM cross-coupling/ nitro hydrogenation reactions under optimized is shown in figure 16.

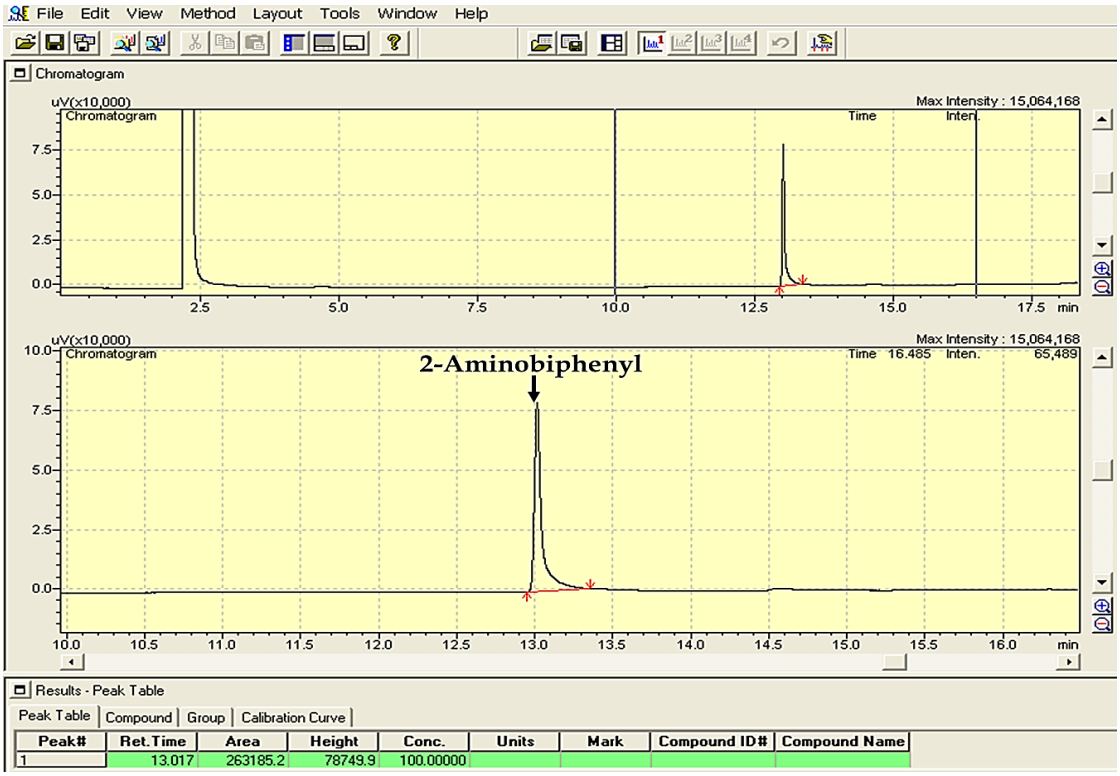

Figure 16. Gas chromatograph of Tandem SM cross-coupling/ nitro hydrogenation

Control experiment

In order to understand the role of each component in synthesized material, control experiments were carried out with ZrO_2, PMo_{12}, PMo_{12}/ZrO_2, $PdCl_2$, Pd/ZrO_2 and $Pd\text{-}PMo_{12}/ZrO_2$ under optimized conditions for SM cross-coupling as well as Tandem Suzuki-Miyaura cross-coupling/ nitro hydrogenation reaction. From Table 5 it can be seen that the ZrO_2, PMo_{12} and PMo_{12}/ZrO_2 are inactive towards both the reaction, this further confirms that PMo_{12} act as a stabilizing agent for Pd as we have already mentioned in introduction. However, we obtained almost same % conversion and selectivity for both the reactions, when carried out with $PdCl_2$ and Pd/ZrO_2 having same active amount of Pd. Obtained results confirmed the Pd is the only active reactive species for the progress of reaction.

Table 5. Control experiment

Catalyst	% [a]Conversion	% [b]Conversion	% Selectivity	
			C-C coupling	NO_2 hydrogenation
ZrO_2	NA	NA	NA	NA
PMo_{12}	NA	NA	NA	NA
PMo_{12}/ZrO_2	NA	NA	NA	NA
$PdCl_2$	92	100	4	96
Pd/ZrO_2	96	100	7	93
$Pd\text{-}PMo_{12}/ZrO_2$	>99	100	NA	99

[a]Reaction conditions for SM cross-coupling: catalyst (ZrO_2;15.38 mg, PMo_{12}; 4.62 mg, PMo_{12}/ZO_2; 19.1 mg), 1-iodo-2-nitrobenzene (1.96 mmol), phenylboronic acid (2.94 mmol), EtOH: H_2O (5:5 mL), K_2CO_3 (3.96 mmol), time (1.5 h) and temperature (90 °C).

[b]Reaction conditions for Tandem: catalyst (ZrO_2;38.45 mg, PMo_{12}; 11.5 mg, PMo_{12}/ZO_2; 47.75 mg), 1-iodo-2-nitrobenzene (1.96 mmol), phenylboronic acid (2.94 mmol), EtOH: H_2O (5:5 mL), K_2CO_3 (3.96 mmol), pressure (10 bar), time (24 h) and temperature (90 °C).

Hot filtration and heterogeneity test

In heterogeneous catalysis, one of the most basic requirements is that the catalyst should retain its heterogeneity up to several cycles with its active sites intact. In order to check leaching of Pd from Pd-PMo_{12}/ZrO_2 and Pd/ZrO_2 in both reactions, hot filtration test was carried out. In case of SM cross-coupling reaction, initially reaction was performed up to 45 min with Pd-PMo_{12}/ZrO_2 and Pd/ZrO_2, afterward both catalysts were removed from hot reaction mass and reaction was further proceed for 45 min (total 90 min). Similarly, in Tandem Suzuki-Miyaura cross-coupling/nitro hydrogenation reaction was carried out using both the same catalysts up to 16 h. After that both the catalysts were removed and reaction was continued up to 24 h (another 8 h). After completion of the reactions, organic layer was extracted by using dichloromethane and analysed by Gas chromatogram.

In case of Pd/ZrO_2 obtained results (Table 6) show rise in conversion by 8% in of SM cross-coupling reaction after removal of catalyst. Whereas, in Tandem reaction no change in % conversion was observed, but 6% rise in selectivity of NO_2 hydrogenation after removal of catalyst was observed. The obtained result from both the reactions indicates that leaching of Pd from the support during reaction. However, Pd-PMo_{12}/ZrO_2 showed no change in % conversion after the removal of catalyst in both the reactions, which confirms that the Pd single atom does not leach out during the reaction. Further heterogeneity of Pd-PMo_{12}/ZrO_2, was confirmed by EDX analysis of regenerated catalyst. Retention of Pd content (0.45 wt%) indicated Pd SACs is stabilized by PMo_{12} over the surface of ZrO_2. These obtained results confirmed the true heterogeneous nature of the catalyst, which is also reflected in recycling study.

Table 6. Hot filtration and heterogeneity test

Catalyst	% [a]Conversion	% [b]Conversion	% Selectivity	
			C-C coupling	NO_2 hydrogenation
Pd/ZrO_2	43(after 1 h)	100 (after 16 h)	41	59
	51 (after 2 h)	100 (after 24 h)	36	64
$Pd\text{-}PMo_{12}/ZrO_2$	51 (after 1 h)	100 (after 16 h)	46	56
	52 (after 2 h)	100 (after 24 h)	46	56

[a]Reaction conditions for SM corss-coupling: catalyst (20 mg), 1-iodo-2-nitrobenzene (1.96 mmol), phenylboronic acid (2.94 mmol), EtOH: H_2O (5:5 mL), K_2CO_3 (3.96 mmol), time (1.5 h) and temperature (90 °C).

[b]Reaction conditions for Tandem: catalyst (50 mg), 1-iodo-2-nitrobenzene (1.96 mmol), phenylboronic acid (2.94 mmol), K_2CO_3 (3.96 mmol), EtOH: H_2O (5:5 mL), pressure (10 bar), time (24 h) and temperature (90 °C).

Regeneration and recycling studies

For any chemical process, sustainability of the catalyst up to several cycles is one of the key issue. Taking this into consideration, after completion of the reaction, the $Pd\text{-}PMo_{12}/ZrO_2$ was regenerated in both reactions through centrifugation and washed with dichloromethane followed by water and finally air-dried to reuse for the next catalytic run. From Table 7, obtained results showed consistent catalytic activity up to three cycles for the both reactions and can be reused for further cycles which depends on choice of the chemist. This clearly shows that the synthesized catalyst is truly heterogeneous in nature.

Table 7. Recycling studies

Catalyst	% [a]Conversion	% [b]Conversion	% Selectivity	
			C-C coupling	NO_2 hydrogenation
Fresh	>99	100	NA	99
R-1	99	100	NA	99
R-2	99	100	NA	99
R-3	99	100	2	98

[a]Reaction conditions for SM corss-coupling: catalyst (20 mg), 1-iodo-2-nitrobenzene (1.96 mmol), phenylboronic acid (2.94 mmol), EtOH: H_2O (5:5 mL), K_2CO_3 (3.96 mmol), time (1.5 h) and temperature (90 °C).

[b]Reaction conditions for Tandem: catalyst (50 mg), 1-iodo-2-nitrobenzene (1.96 mmol), phenylboronic acid (2.94 mmol), K_2CO_3 (3.96 mmol), EtOH: H_2O (5:5 mL), pressure (10 bar), time (24 h) and temperature (90 °C).

Characterization of regenerated catalyst

In order to check sustainability of catalyst, regenerated catalyst (Regenerated Pd-Pmo_{12}/ZrO_2) was characterised by EDX, FT-IR, XPS and powder XRD.

Elemental mapping of regenerated Pd-PMo_{12}/ZrO_2 (Figure 17) is confirmed the presence of all the elements. The found EDX values of Pd (0.44 %wt) and Mo (15.08 %wt) for regenerated Pd-PMo_{12}/ZrO_2, are in good agreement with the fresh one (0.72 wt% Pd and 15.19 wt% Mo), which confirms that there was no leaching of Pd atoms from the catalyst during the reaction.

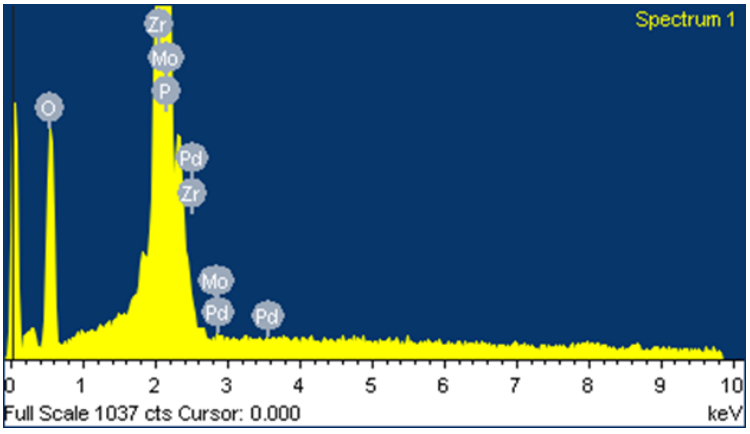

Figure 17. EDX mapping of regenerated Pd-PMo_{12}/ZrO_2

FT-IR spectra of regenerated and fresh Pd-PMo_{12}/ZrO_2 catalysts are displayed in figure 18, which is almost identical with fresh catalyst without any significant shift in the bands. This indicates the retention of catalyst structure even after regeneration of the catalyst. However, the regenerated catalyst shows bands with slight low intensity in as compared to the fresh one, this may be due to the sticking of the substrates on the catalyst, but it had no effect on the efficiency of the catalyst.

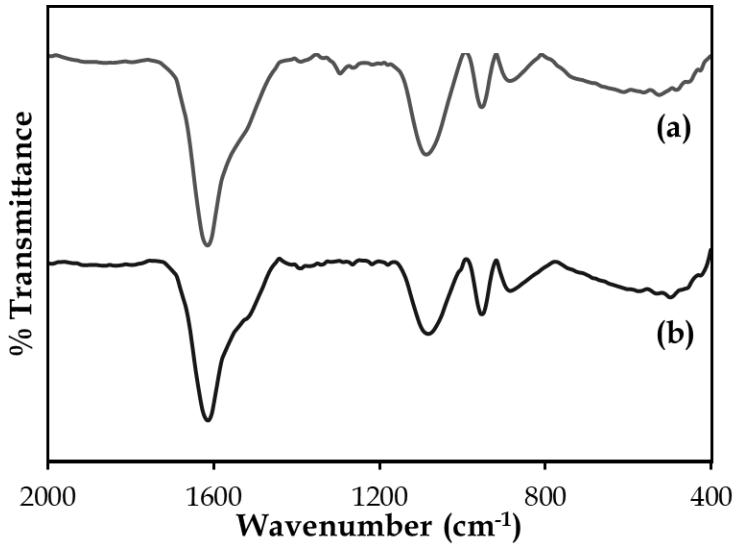

Figure 18. FT-IR spectra of (a) fresh and (b) regenerated Pd-PMo_{12}/ZrO_2

Figure 19 shows the XPS of regenerated Pd-PMo_{12}/ZrO_2. Its consist of all characteristic peaks of Pd, Mo, Zr and O, which are identical to those obtained for fresh catalyst (Figure 6). It further confirms no reduction of Mo (VI) as well as retentions of active Pd SACs on the catalyst surface, thus confirming the sustainability of catalyst.

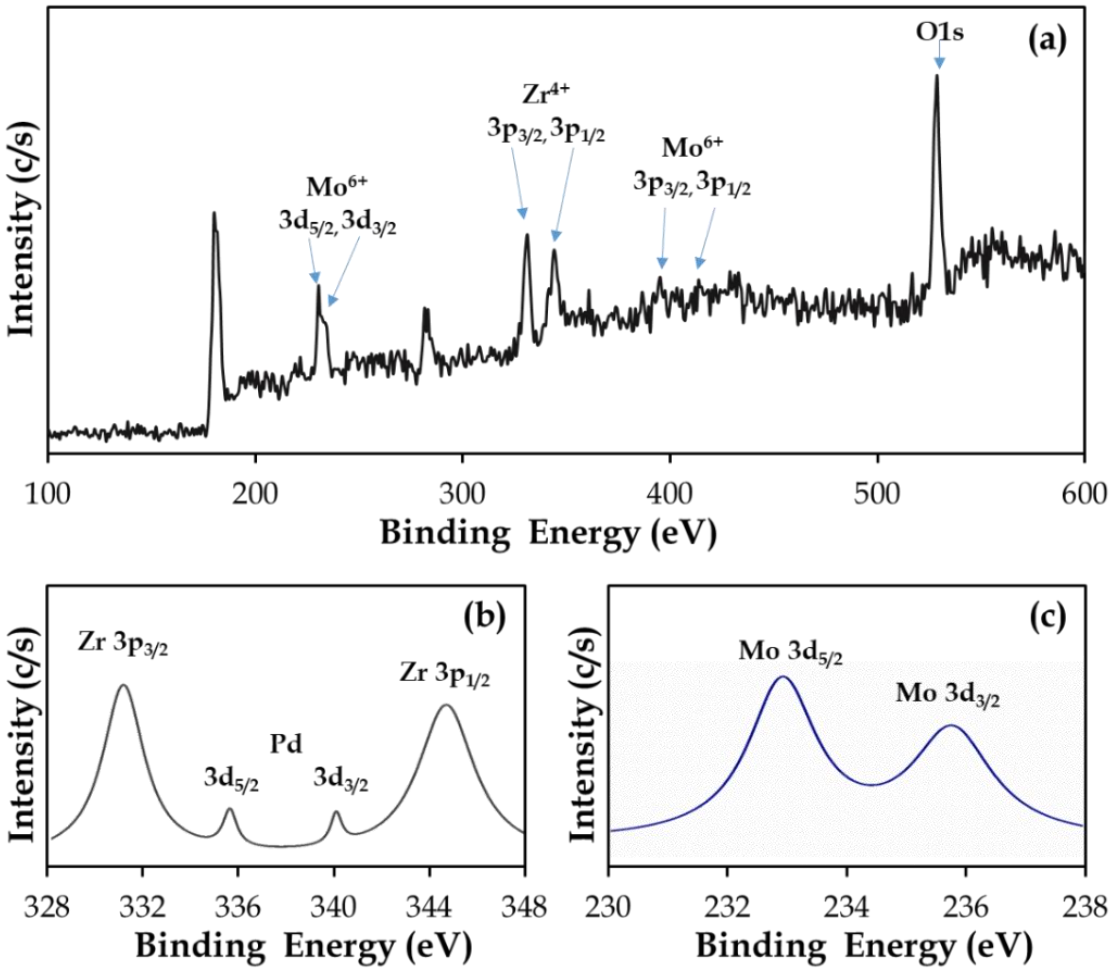

Figure 19. XPS spectra of regenerated Pd-PMo_{12}/ZrO_2

The regenerated Pd-PMo_{12}/ZrO_2 show similar powder XRD patent as fresh catalyst (Figure 20). The obtained result shows the retention of high dispersed nature of the catalyst which further confirm the sustainability of the catalyst.

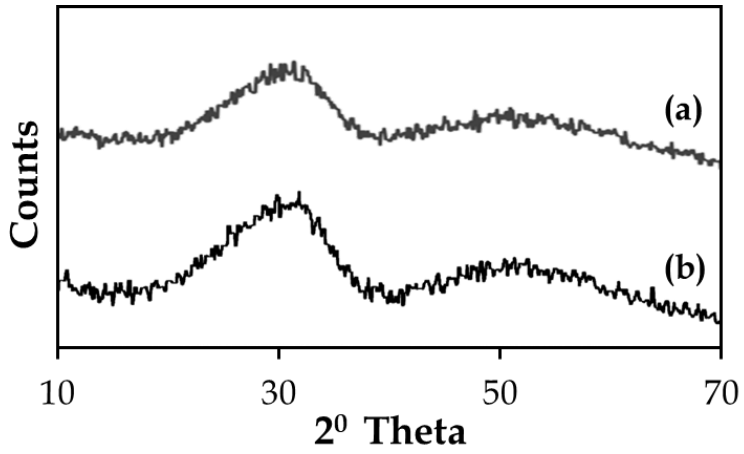

Figure 20. Powder XRD spectra of (a) fresh and (b) regenerated Pd-PMo_{12}/ZrO_2

Mechanistic investigation

In present work, we propose the well-reported mechanism (scheme 4) for mechanistically two different catalytic transformations reactions: i) SM C-C [71, 79] and ii) nitro hydrogenation [80] in reaction. The SM C-C reaction involves oxidative addition, transmetallation and reductive elimination while in the case of nitro hydrogenation reaction we proposed universal hydride transfer via heterolytic cleavage of H_2. In case of reaction, as we have mentioned in "on-water" effect on SM C-C, organopalladium (II) species is formed in organic phase via oxidative addition of Pd SACs atom with 1-iodo-2-nitrobenzene. While in water phase, boron-ate complex is formed by ionization of phenyl boronic acid in higher basic water phase (formed by K_2CO_3). Afterwards at water-organic interphase, organopalladium species undergo transmetallation with boron-ate complex to produce a new organopalladium complex by replacing the phenyl ring of phenylboronic acid with halides of organopalladium spices. Finally, product (2-nitrobiphenyl) was formed and Pd(0) SACs was regenerated for further hydrogenation reaction. For hydrogenation reaction after applying H_2 pressure, initially hydrogen gets adsorbed on Pd atom to form Pd-H by heterolytic cleavage of H_2 followed by adsorption of 2-nitrobiphenyl on Pd-H surface of catalyst by electrostatic interactions to form an anionic N,N-dihydroxylamine via hydride transfer. This was further followed by protonation to yield N,N-dihydroxylamine intermediate by eliminating water molecule, which gets dehydrated to generate 2-nitrosobiphenyl. The nitroso group in 2-nitrosobiphenyl is further attacked by hydride of Pd-H and protonated to yield N-hydroxylamine, which further is protonated followed hydride transfer to form 2-aminobiphenyl and the catalyst was regenerated for the next catalytic cycle.

Further, for nitro hydrogenation reaction step, to confirm the formation of nitroso intermediates, a set of reactions, after completion of SM C-C reaction H_2 pressure was applied for two, six and ten hours and obtained reaction mass

was analysed by GC. The result shows 100% conversion with only 2%, 11% and 21% selectivity of 2-aminobiphenyl in 2, 6 and 10 h respectively, and no other peak corresponding to 2-nitrosobiphenyl was found. This indicates that formed 2-nitrosobiphenyl intermediate is unstable and difficult to isolate. To further confirm this, reaction mass obtained after 10 hrs was analysed by ^{1}H NMR and the spectra show peaks correspond to 2-nitrobiphenyl (Figure 21) and 2-aminobiphenyl (Figure 22) but does not show any peak corresponding to 2-nitrosobipheny (Figure 23). The absence of peak corresponding to nitroso intermediate shows that the intermediate is unstable and immediately converts to form amine. If not so, we should get some additional peak in NMR. The above study clearly indicates that the intermediate is highly unstable and hence difficult to isolate during from the reaction mixture.

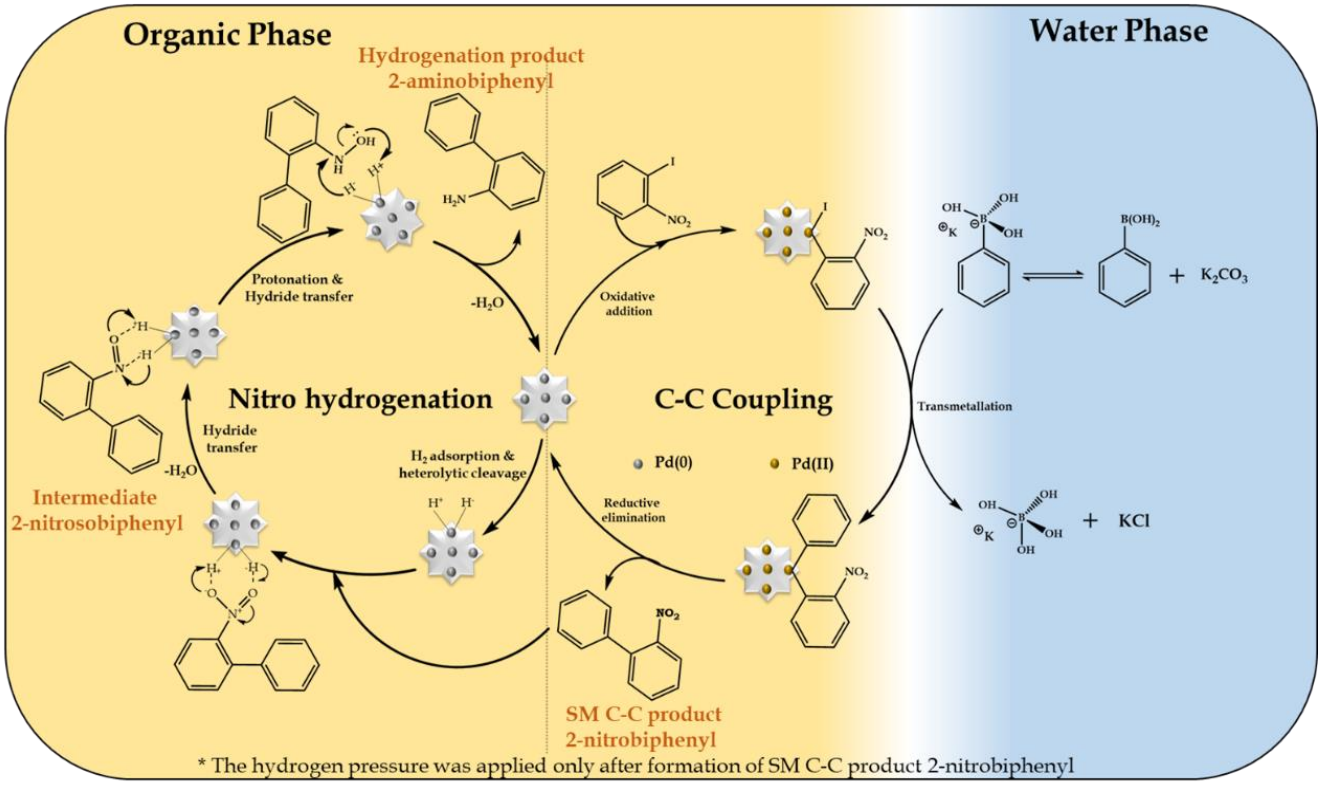

Scheme 4. Plausible Suzuki-Miyaura cross-coupling/ nitro hydrogenation reaction

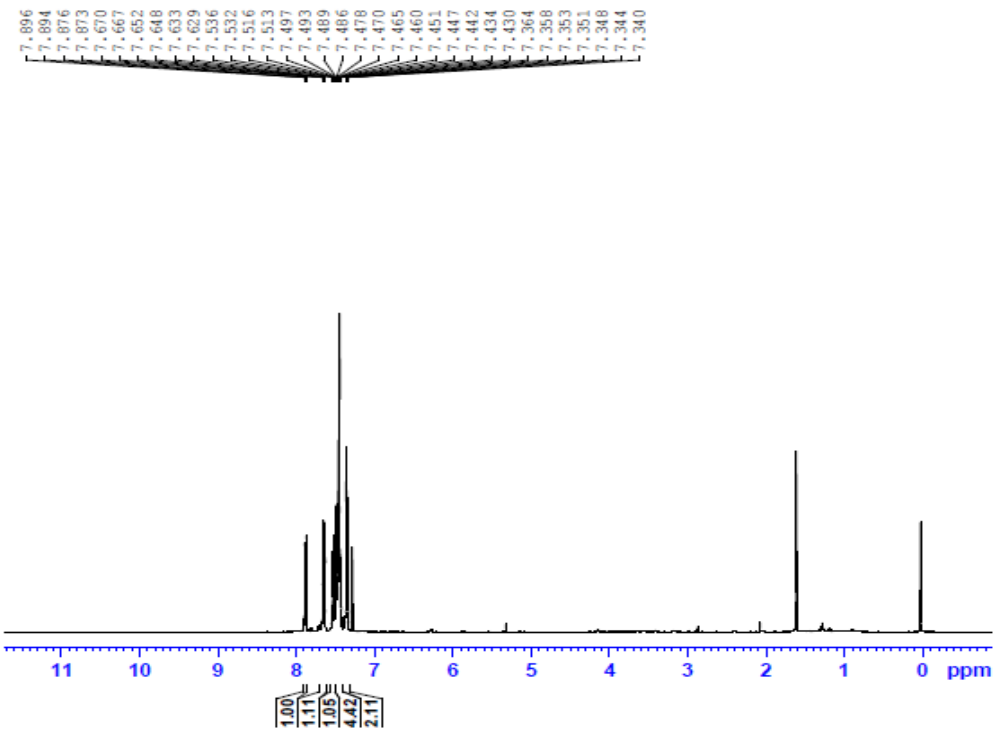

Figure 21. ^{1}H NMR of 2-nitrobiphenyl

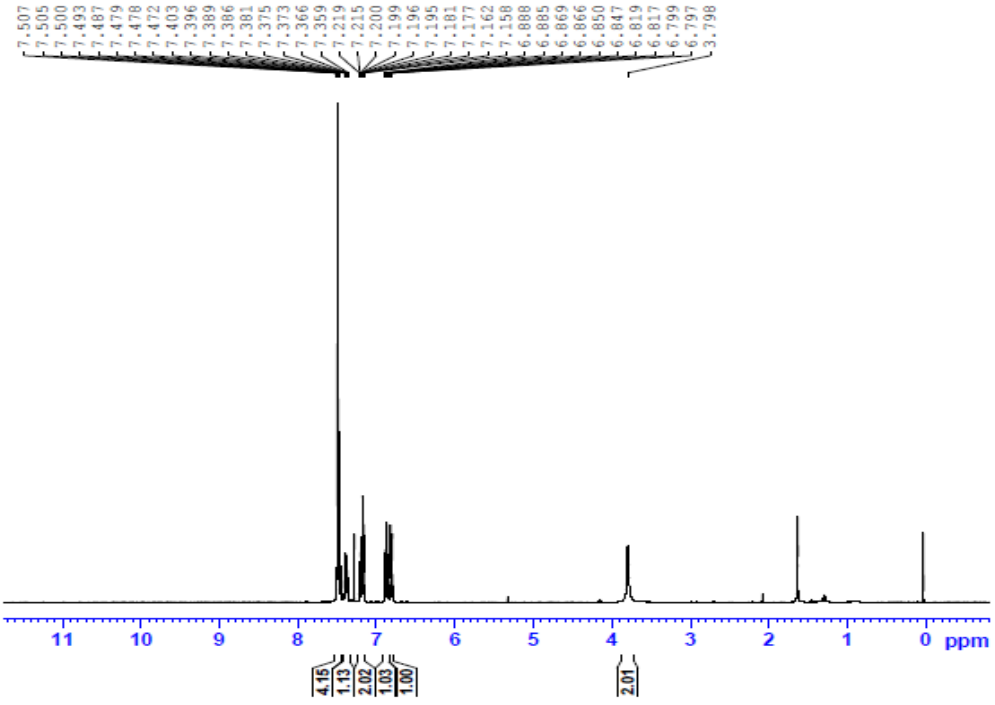

Figure 22. ^{1}H NMR of 2-aminobiphenyl

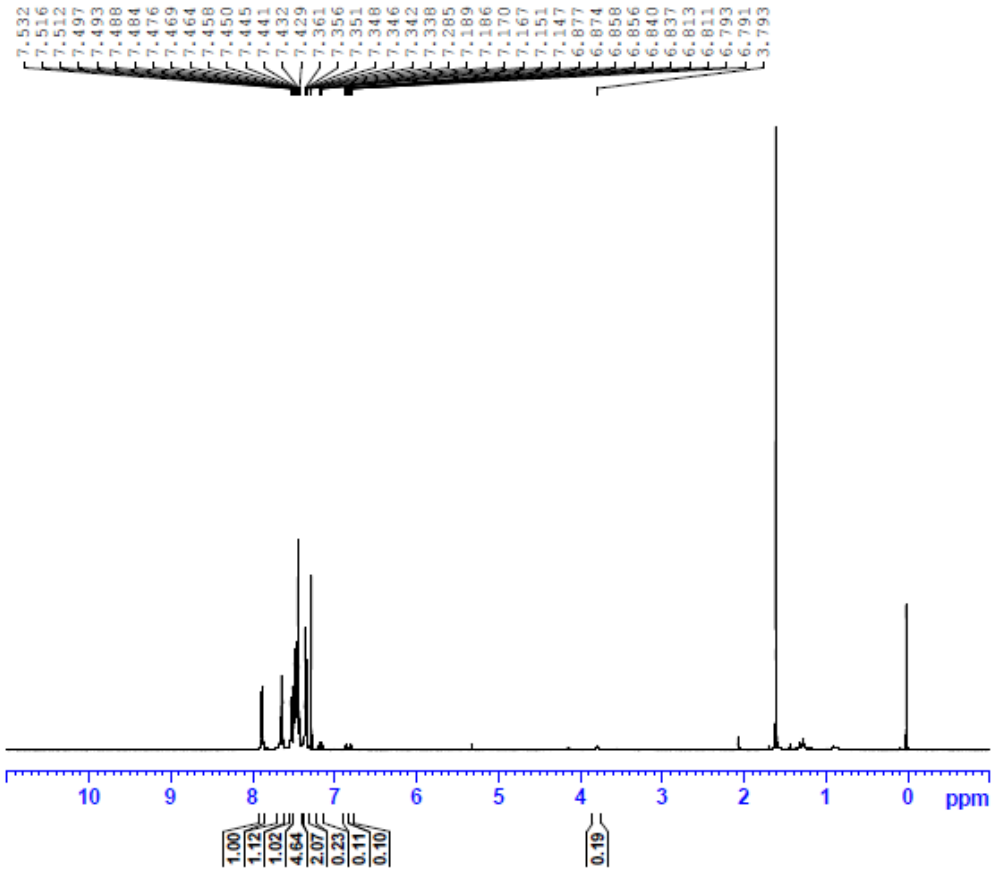

Figure 23. ^{1}H NMR of 10 h reaction mass

CONCLUSION

- **Pd SASc stabilized** by **phosphomolybdic acid** supported on **zirconia** was successfully designed and characterized by various physicochemical techniques.
- **XPS** confirmed the **metallic state of Pd** whereas **HRTEM and HAADF-STEM** revealed the isolative dispersion of **Pd SASc onto the surface of PMo_{12}/ZrO_2.**
- The catalyst exhibited outstanding catalytic **activity (100% conversion and 99% selectivity for 2-aminobiphenyl)** for tandem Suzuki–Miyaura cross-coupling/nitro hydrogenation reaction under mild reaction conditions in **aqueous medium, ethanol–water.**
- The **true heterogeneous nature** of the catalyst was confirmed by the **hot filtration method.**
- The **regenerated** and **recycling study shows stable catalytic activity** up to **three runs** (and can be used for more), whereas sustainability of catalyst was confirmed by the characterization of **regenerated catalyst**.

Comparison of study $PMo_{11}Pd$ and Pd-PMo_{12}/ZrO_2

In order to check the activity order, hydrogenation and tandem Suzuki–Miyaura cross-coupling/nitro hydrogenation reactions were carried out by $PMo_{11}Pd$ and Pd-PMo_{12}/ZrO_2 using similar active amount of Pd under identical experimental conditions and obtained results are compared in terms of % conversion and selectivity.

Table 8. LA hydrogenation and tandem Suzuki–Miyaura cross-coupling/nitro hydrogenation in identical condition

Catalyst	LA hydrogenation	Suzuki–Miyaura cross-coupling/nitro hydrogenation		
	% Conversion	% Conversion	% Selectivity	
			C-C coupling	NO_2 hydrogenation
$PMo_{11}Pd$	95	100	8	92
Pd-PMo_{11}/ZrO_2	98	100	NA	99

Reaction conditions for LA hydrogention: Catalyst (Pd: $1.879*10^{-3}$ mmol), substrate/catalyst ratio (2661), LA (5 mmol), FA (125 mmol), time (6 h) and temperature (200 °C).

Reaction conditions for tandem Suzuki–Miyaura cross-coupling/nitro hydrogenation: Catalyst (Pd: $2.066*10^{-3}$ mmol), substrate/catalyst ratio (949) 1-iodo-2-nitrobenzene (1.96 mmol), phenylboronic acid (2.94 mmol), EtOH: H_2O (5:5 mL), K_2CO_3 (3.96 mmol), pressure (10 bar), time (24 h) and temperature (90 °C).

From the table 8, it is seen that Pd-PMo_{12}/ZrO_2 is more active as compared to $PMo_{11}Pd$ for LA hydrogenation as well as tandem Suzuki–Miyaura cross-coupling/nitro hydrogenation reaction. This can be explained on the basis of structural diversity of substrate and catalytically active Pd position in the designed catalyst (Figure 24). In case of LA hydrogenation, active Pd site is present in lacuna in $PMo_{11}Pd$ (Figure 24a) by removing one M=O unit, which can be difficult approach for carbonyl C=O present in LA (Figure 24b) as compared to the catalytic active species where Pd is present Pd-PMo_{12}/ZrO_2

(Figure 24c) at counter cation position by exchanging available protons of PMo_{12} (as secondary structure).

Similarly, in tandem Suzuki–Miyaura cross-coupling/nitro hydrogenation reaction, 2-nitrobiphenyl (Figure 24d) is formed after Suzuki–Miyaura cross-coupling reaction, which can be further easily approached for NO_2 hydrogenation for Pd-PMo_{12}/ZrO_2 as compared to $PMo_{11}Pd$ as mentioned above as well as due to the structure diversity of 2-nitrobiphenyl, which is well known.

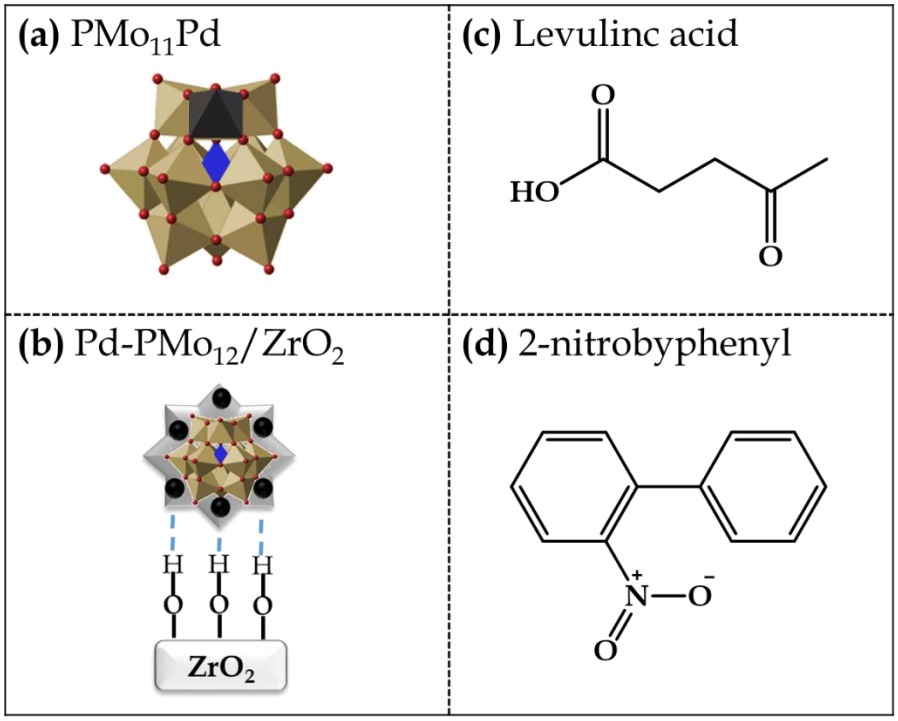

Figure 24. (a) structure of levulinic acid (LA), (b) structure of 2-nitrobyphenyl, (c) $PMo_{11}Pd$ (Lacunary) and (d)Pd-PMo_{12}/ZrO_2

REFERENCES

[1] D. Pan, J. Chen, W. Tao, L. Nie, S. Yao, Langmuir, 22, 5872, (2006).

[2] M. J. F. Guinel, A. Bonakdarpour, B. Wang, P. K. Babu, F. Ernst, N. Ramaswamy, S. Mukerjee, A. Wieckowski, ChemSusChem, 2, 658, (2009).

[3] H. Li, X. Zhang, H. Pang, C. Huang, J. Chen, J. Solid State Electrochem., 14, 2267, (2010).

[4] Z. Cui, C. M. Li, S. P. Jiang, Phys. Chem. Chem. Phys., 13, 16349, (2011).

[5] Y. Li, X. Yang, F. Yang, Y. Wang, P. Zheng, X. Liu, Electrochim. Acta, 66, 188, (2012).

[6] X. Jin, B. He, J. Miao, J. yuan, Q. Zhang, L. Niu, Carbon, 50, 3083, (2012).

[7] M. H. Seo, S. M. Choi, H. J. Kim, J. H. Kim, B. K. Cho, W. B. Kim, J. Power Sources., 179, 81, (2008).

[8] Z. Cui, W. Xing, C. Liu, D. Tian, H. Zhang, J. Power Sources., 195, 1619, (2010).

[9] S. Li, X. Yu, G. Zhang, Y. Ma, J. Yao, P. de Oliveira, Carbon, 49, 1906, (2011).

[10] Z. Bai, C. Zhou, N. Gao, H. Pang, H. Ma, RSC Adv., 6, 937, (2016).

[11] F. Amouzad, K. Zarei, J. Electron. Mater., 49, 3583, (2020).

[12] X. Zhao, J. Zhu, L. Liang, C. Liu, J. Liao, W. Xing, J. Power Sources., 210, 392, (2012).

[13] M. Zhu, X. Gao, G. Luo, B. Dai, J. Power Sources., 225, 27, (2013).

[14] A. Ma, X. Zhang, X. Wang, L. Le, S. Lin, RSC Adv., 5, 64534, (2015).

[15] J. S. Li, H. Q. Dong, S. L. Li, R. H. Li, Z. H. Dai, J. C. Bao, Y. Q. Lan, New J. Chem., 40, 914, (2016).

[16] S. Zoladek, I. A. Rutkowska, M. Blicharska, K. Miecznikowski, W. Ozimek, J. Orlowska, E. Negro, V. Di Noto, P. J. Kulesza, Electrochim. Acta, 233, 113, (2017).

[17] A. A. Novikov, A. R. Sayfutdinova, M. V. Gorbachevskii, S. V. Filatova, A. V. Filimonova, U. P. Rodrigues-Filho, Y. Fu, W. Wang, H. Wang, V. A. Vinokurov, D. G. Shchukin, ACS Omega, 7, 6728, (2022).

[18] C. Copéret, A. Comas-Vives, M. P. Conley, D. P. Estes, A. Fedorov, V. Mougel, H. Nagae, F. Núñez-Zarur, P. A. Zhizhko, Chem. Rev., 116, 323, (2016).

[19] N. Zhang, C. Ye, H. Yan, L. Li, H. He, D. Wang, Y. Li, Nano Res., 13, 3165, (2020).

[20] C. Gao, J. Low, R. Long, T. Kong, J. Zhu, Y. Xiong, Chem. Rev., 120, 12175, (2020).

[21] Y. Liu, X. Wu, Z. Li, J. Zhang, S.-X. Liu, S. Liu, L. Gu, L. R. Zheng, J. Li, D. Wang, Y. Li, Nat. Commun., 12, 4205, (2021).

[22] X. F. Yang, A. Wang, B. Qiao, J. Li, J. Liu, T. Zhang, Acc. Chem. Res., 46, 1740, (2013).

[23] H. Yang, L. Shang, Q. Zhang, R. Shi, G. I. N. Waterhouse, L. Gu, T. Zhang, Nat. Commun., 10, 4585, (2019).

[24] M. Flytzani-Stephanopoulos, B. C. Gates, Annu. Rev. Chem. Biomol. Eng., 3, 545, (2012).

[25] V. Muravev, G. Spezzati, Y.-Q. Su, A. Parastaev, F.-K. Chiang, A. Longo, C. Escudero, N. Kosinov, E. J. Hensen, Nat. Catal., 4, 469, (2021).

[26] L. Liu, A. Corma, Chem. Rev., 118, 4981, (2018).

[27] B. Zhang, H. Asakura, J. Zhang, J. Zhang, S. De, N. Yan, A Angew. Chem. Int. Ed., 55, 8319, (2016).

[28] B. Zhang, G. Sun, S. Ding, H. Asakura, J. Zhang, P. Sautet, N. Yan, J. Am. Chem. Soc., 141, 8185, (2019).

[29] Y. Cheng, S. Zhao, B. Johannessen, J.-P. Veder, M. Saunders, M. R. Rowles, M. Cheng, C. Liu, M. F. Chisholm, R. De Marco, H.-M. Cheng, S.-Z. Yang, S. P. Jiang, Adv. Energy Mater., 30, 1706287, (2018).

[30] L. Wang, M. X. Chen, Q. Q. Yan, S. L. Xu, S. Q. Chu, P. Chen, Y. Lin, H. W. Liang, Sci. Adv., 5, eaax6322, (2019).

[31] R. Liu, C. Streb, Adv. Energy Mater., 11, 2101120, (2021).

[32] X. He, Q. He, Y. Deng, M. Peng, H. Chen, Y. Zhang, S. Yao, M. Zhang, D. Xiao, D. Ma, B. Ge, H. Ji, Nat. Commun., 10, 3663, (2019).

[33] S. Vajda, M. G. White, ACS Catal. 5, 7152, (2015).

[34] J. Wan, W. Chen, C. Jia, L. Zheng, J. Dong, X. Zheng, Y. Wang, W. Yan, C. Chen, Q. Peng, D. Wang, Y. Li, Adv. Mater., 30, 1705369, (2018).

[35] H. Wei, K. Huang, D. Wang, R. Zhang, B. Ge, J. Ma, B. Wen, S. Zhang, Q. Li, M. Lei, C. Zhang, J. Irawan, L.-M. Liu, H. Wu, Nat. Commun., 8, 1490, (2017).

[36] S. Liu, J. M. Tan, A. Gulec, L. A. Crosby, T. L. Drake, N. M. Schweitzer, M. Delferro, L. D. Marks, T. J. Marks, P. C. Stair, Organometallics, 36, 818, (2017).

[37] F. R. Lucci, J. Liu, M. D. Marcinkowski, M. Yang, L. F. Allard, M. Flytzani-Stephanopoulos, E. C. H. Sykes, Nat. Commun., 6, 8550, (2015).

[38] J. Jones, H. Xiong, A. T. DeLaRiva, E. J. Peterson, H. Pham, S. R. Challa, G. Qi, S. Oh, M. H. Wiebenga, X. I. Pereira Hernández, Y. Wang, A. K. Datye, Science, 353, 150, (2016).

[39] Y. Chen, S. Ji, Y. Wang, J. Dong, W. Chen, Z. Li, R. Shen, L. Zheng, Z. Zhuang, D. Wang, Y. Li, Angew. Chem. Int. Ed., 56, 6937, (2017).

[40] L. Jiao, G. Wan, R. Zhang, H. Zhou, S.-H. Yu, H.-L. Jiang, Angew. Chem. Int. Ed., 57, 8525, (2018).

[41] J. Shan, M. Li, L. F. Allard, S. Lee, M. Flytzani-Stephanopoulos, Nature, 551, 605, (2017).

[42] C. Zhao, X. Dai, T. Yao, W. Chen, X. Wang, J. Wang, J. Yang, S. Wei, Y. Wu, Y. Li, J. Am. Chem. Soc., 139, 8078, (2017).

[43] B. Qiao, A. Wang, X. Yang, L. F. Allard, Z. Jiang, Y. Cui, J. Liu, J. Li, T. Zhang, Nat. Chem., 3, 634, (2011).

[44] X. Guo, G. Fang, G. Li, H. Ma, H. Fan, L. Yu, C. Ma, X. Wu, D. Deng, M. Wei, D. Tan, R. Si, S. Zhang, J. Li, L. Sun, Z. Tang, X. Pan, X. Bao, Science, 344, 616, (2014).

[45] P. Liu, Y. Zhao, R. Qin, S. Mo, G. Chen, L. Gu, D. M. Chevrier, P. Zhang, Q. Guo, D. Zang, B. Wu, G. Fu, N. Zheng, Science, 352, 797, (2016).

[46] Z. Zhang, Y. Zhu, H. Asakura, B. Zhang, J. Zhang, M. Zhou, Y. Han, T. Tanaka, A. Wang, T. Zhang, N. Yan, Nat. Commun., 8, 16100, (2017).

[47] R. Lang, W. Xi, J.-C. Liu, Y.-T. Cui, T. Li, A. F. Lee, F. Chen, Y. Chen, L. Li, L. Li, J. Lin, S. Miao, X. Liu, A.-Q. Wang, X. Wang, J. Luo, B. Qiao, J. Li, T. Zhang, Nat. Commun., 10, 234, (2019).

[48] H. Wang, Q. Wang, Y. Cheng, K. Li, Y. Yao, Q. Zhang, C. Dong, P. Wang, U. Schwingenschlögl, W. Yang, X. X. Zhang, Nano Lett., 12, 141, (2012).

[49] S. Sun, G. Zhang, N. Gauquelin, N. Chen, J. Zhou, S. Yang, W. Chen, X. Meng, D. Geng, M. N. Banis, R. Li, S. Ye, S. Knights, G. A. Botton, T.-K. Sham, X. Sun, Sci. Rep., 3, 1775, (2013).

[50] L. Zhang, Y. Jia, G. Gao, X. Yan, N. Chen, J. Chen, M. T. Soo, B. Wood, D. Yang, A. Du, X. Yao, Chem, 4, 285, (2018).

[51] F. Huang, Y. Deng, Y. Chen, X. Cai, M. Peng, Z. Jia, J. Xie, D. Xiao, X. Wen, N. Wang, Z. Jiang, H. Liu, D. Ma, Nat. Commun., 10, 4431, (2019).

[52] S. Cao, H. Li, T. Tong, H.-C. Chen, A. Yu, J. Yu, H. M. Chen, Adv. Funct. Mater., 28, 1802169, (2018).

[53] J. Gu, C.-S. Hsu, L. Bai, H. M. Chen, X. Hu, Science, 364, 1091, (2019).

[54] T. Sun, Y. Li, T. Cui, L. Xu, Y.-G. Wang, W. Chen, P. Zhang, T. Zheng, X. Fu, S. Zhang, Z. Zhang, D. Wang, Y. Li, Nano Lett., 20, 6206, (2020).

[55] J. Zhang, C. Zheng, M. Zhang, Y. Qiu, Q. Xu, W.-C. Cheong, W. Chen, L. Zheng, L. Gu, Z. Hu, D. Wang, Y. Li, Nano Res., 13, 3082, (2020).

[56] Q. He, D. Liu, J. H. Lee, Y. Liu, Z. Xie, S. Hwang, S. Kattel, L. Song, J. G. Chen, Angew. Chem. Int. Ed., 59, 3033, (2020).

[57] S. Tian, M. Hu, Q. Xu, W. Gong, W. Chen, J. Yang, Y. Zhu, C. Chen, J. He, Q. Liu, H. Zhao, D. Wang, Y. Li, Science China Mater., 64, 642, (2021).

[58] J. Wang, Z. Huang, W. Liu, C. Chang, H. Tang, Z. Li, W. Chen, C. Jia, T. Yao, S. Wei, Y. Wu, Y. Li, J. Am. Chem. Soc., 139, 17281, (2017).

[59] Z. Liang, C. Qu, D. Xia, R. Zou, Q. Xu, Angew. Chem. Int. Ed., 57, 9604, (2018).

[60] T. Sun, L. Xu, D. Wang, Y. Li, Nano Res., 12, 2067, (2019).

[61] C. Wan, X. Duan, Y. Huang, Adv. Energy Mater., 10, 1903815, (2020).

[62] M. Babucci, A. Guntida, B. C. Gates, Chem. Rev., 120, 11956, (2020).

[63] Y. Liu, Z. Li, Q. Yu, Y. Chen, Z. Chai, G. Zhao, S. Liu, W. C. Cheong, Y. Pan, Q. Zhang, L. Gu, L. Zheng, Y. Wang, Y. Lu, D. Wang, C. Chen, Q. Peng, Y. Liu, L. Liu, J. Chen, Y. Li, J. Am. Chem. Soc., 141, 9305, (2019).

[64] H. S. Wang, Y. C. Wang, Y. M. Pan, S. L. Zhao, Z. F. Chen, Tetrahedron Lett., 49, 2634, (2008).

[65] A. Qazi, A. Sullivan, Dalton Trans., 40, 10637 (2011).

[66] A. Kumar, K. Purkait, S. K. Dey, A. Sarkar, A. Mukherjee, RSC Adv., 4, 35233, (2014).

[67] S. Rohilla, P. Pant, N. Jain, RSC Adv., 5, 31311, (2015).

[68] B. S. Kumar, A. J. Amali, K. Pitchumani, J. Mol. Catal. A: Chem., 423, 511, (2016).

[69] A. Kunfi, Z. May, P. Németh, G. London, J. Catal., 361, 84, (2018).

[70] A. Patel, A. Patel, Catal. Lett., 148, 3534, (2018).

[71] A. Patel, A. Patel, Catal. Lett., 149, 1476, (2019).

[72] A. Patel, A. Patel, RSC Adv., 11, 8218, (2021).

[73] N. Mizuno, J.-S. Min, A. Taguchi, Chem. Mater., 16, 2819, (2004).

[74] X. Zhang, Q. Chen, D. C. Duncan, R. J. Lachicotte, C. L. Hill, Inorg. Chem., 36, 4381, (1997).

[75] Y. Zhu, W. D. Wang, X. Sun, M. Fan, X. Hu, Z. Dong, ACS Appl. Mater. Interfaces, 12, 7285, (2020).

[76] P. Singh, S. Mishra, A. Sahoo, S. Patra, Scientific Reports, 11, 9305, (2021).

[77] M. Liu, H. Yang, Z. Xu, W. Ma, F. Cui, G. Lu, L. Xu, T. Cui, New J. Chem., 44, 7035, (2020).

[78] M. Wang, H. Xue, F. Ju, H. Yang, Sci. Rep., 7, 7006, (2017).

[79] P. Orecchia, D. S. Petkova, R. Goetz, F. Rominger, A. S. K. Hashmi, T. Schaub, Green Chem., 23, 8169, (2021).

[80] S. I. El-Hout, S. M. El-Sheikh, H. M. A. Hassan, F. A. Harraz, I. A. Ibrahim, E. A. El-Sharkawy, Appl. Catal. A: Gen., 503, 176, (2015).